Magnetic effects on the Chern Kondo insulator

Sen Niu and Xiong-Jun Liu*
International Center for Quantum Materials and School of Physics, Peking University, Beijing 100871, China
and Collaborative Innovation Center of Quantum Matter, Beijing 100871, China

(Received 15 May 2018; revised manuscript received 6 September 2018; published 25 September 2018)

We examine the Chern Kondo insulator proposed in a square optical lattice with staggered flux induced by s-p orbital hybridization by revisiting its realization and taking into account the magnetic effects for the Kondo phases. The Ruderman-Kittel-Kasuya-Yoshida interaction is analyzed at the weak s-p hybridization regime, with the anisotropic magnetic effects being discussed. Furthermore, the paramagnetic and magnetic phases coexisting with Kondo couplings are systematically investigated through the slave-boson theory, for which the rich effects on the Chern Kondo phase are obtained, including the antiferromagnetic, collinear antiferromagnetic Kondo insulator, and Kondo metal phases. The magnetic orders are shown to enhance the effective Kondo hybridization compared with the case without taking into account magnetic effects, and exhibit different influences on the bulk topology. In particular, the antiferromagnetic ordering always enhances the topological phase by increasing the bulk gap of the Chern Kondo phases. The results show the rich topological and magnetic effects obtained in the present Chern Kondo lattice model. We also investigate how to identify the topology and strong correlation effects through measuring the Hall conductance and double occupancy, which are achievable in ultracold atom experiments.

DOI: 10.1103/PhysRevB.98.125141

I. INTRODUCTION

The compound SmB_6, a typical strongly correlated insulator, has recently been predicted to be a time-reversal-invariant topological Kondo insulator (TKI) [1–3], in which the protected conducting surface states account for the saturated resistivity observed in experiment at low-temperature limit [4]. The topological surface states of the proposed TKIs have been observed by experiments [5–14]. On the other hand, there are still interesting topics that remain to be further explored, e.g., the existence of a neutral Fermi surface in the bulk of the TKI SmB_6 [15] motivated by the observation of bulk quantum oscillations [16,17], linear specific heat, anomalous thermal, and optical conductivity [18–21]. While from the effective band description the topology of the TKIs is essentially the same as that of an uncorrelated TI [22], the new effects arising from the electronic correlations in TKIs have been predicted in theory [15,22–29]. Nevertheless, to directly observe the strong correlation effects is typically challenging for condensed matter experiments. Recently, a strongly correlated quantum anomalous Hall (QAH) phase, called Chern Kondo (CK) insulator, was proposed based in the optical lattice [30]. It was shown that both the novel topological physics and the strong correlation effects can be directly measured by taking the advantages of cold atom platforms which are fully controllable and have been broadly applied to explore the exotic topological quantum phases and correlation physics (see, e.g., Refs. [31–49]). In this work, we shall study the magnetic effects on the CK phase, with different physics being predicted.

The original idea of CK insulator [30] is summarized as follows. Consider a checkerboard superlattice with s orbitals on A sites and p_X orbitals on B sites. Due to anisotropy of the superlattice, the nearest-neighbor hopping between p_X orbitals is along the $\hat{X}$ direction and forms an itinerant p_X band, while the nearest-neighbor hopping between s orbitals is along the $\hat{Y}$ direction, forming a nearly flat band and lying below p_X band. Through optical-assisted Feshbach resonance [50–56] the repulsive onsite interaction for s orbitals is tuned to be strong, while the onsite interaction for p_X orbitals is negligible. Without s-p_X hybridization, the s orbitals on A sites form a Mott insulator at half-filling. By laser-assisted tunneling [57–60], the s-p_X hybridization is induced and a periodic Anderson model with laser-induced staggered flux is realized. When the hybridization is tuned to exceed a critical value, the Kondo phase emerges with a finite s-p_X hybridization gap being formed. The gapped quasiparticle band results in a nontrivial correlated Chern insulator with QAH effect [30]. The difference between the noninteracting Chern insulator and CK insulator can be detected by measuring the band topology and double occupancy experimentally.

Nevertheless, there are important issues of the CK insulating phase which were not well addressed in the previous work [30]. First of all, we examine in detail the realization of the Chern insulating phase, and found that the previous scheme is not applicable to generate a staggered flux pattern for the checkerboard lattice, which is essential to realize the Chern insulating phase. Second, in the original work, only the paramagnetic state was considered, while it was shown that in Kondo lattice problems the Ruderman-Kittel-Kasuya-Yoshida (RKKY) interaction between the localized electrons competes with the Kondo effect, resulting in magnetic phases in weak coupling regime [61], and in periodic Anderson

*Corresponding author: xiongjunliu@pku.edu.cn

lattice problems the magnetic instability also occurs in the Kondo phases [62–65]. It is then important to investigate the possible existence of magnetic phases in the CK model, and the effect of magnetism on the CK phase and the phase transition. In this work, we fully address these issues and uncover nontrivial topological Kondo physics which were not predicted previously. In particular, we improve the previous realization and propose a feasible scheme to generate the s-p_X orbital hybridization with a staggered flux which can induce QAH phase in the noninteracting regime. Moreover, we study systematically the magnetic effects on the strongly correlated QAH phase based on RKKY interaction and the slave-boson mean-field theory. We map out the magnetic and QAH phase diagrams, and show that the magnetic orders depend on the s-p_X hybridization strength and the flux ϕ_0 generated by the laser-assisted tunneling. The different magnetic orders can have different influences on QAH phases. Interestingly, a significant enhancement of the correlated QAH effect by the magnetic ordering is predicted.

The structure of this paper is organized as follows. In Sec. II, we examine the realization of the CK model in detail, and propose a feasible scheme for the realization based on the previous one [30]. In Sec. III, we derive the effective Kondo lattice Hamiltonian and RKKY interaction, with which we investigate the magnetic effects controlled by s-p_X hybridization. Section IV presents a systematic study of the ground-state magnetism and QAH phase diagram through the slave-boson theory. Especially, in this section we also study the influences of topology and strong correlation on the CK phase, which can be identified by measuring Hall conductance and double occupancy in cold atom experiments. The conclusions are given in the last Sec. V.

II. IMPROVED SCHEME FOR REALIZATION

In the realization of CK insulator [30], the laser-assisted tunneling is applied to generate the complex s-p_X hybridization which is associated with a staggered magnetic flux. Nevertheless, in Sec. II A we point out that the original laser-assisted tunneling failed to create the required flux, and a modified configuration is necessary. In Sec. II B we improve the original method and propose a feasible scheme for the realization, as shown in Fig. 5 following the method in Ref. [66]. Different from the previous proposal which applies a beam running in the x-y plane to induce Raman transition [30], in our scheme the Raman beam propagates along the $\hat{z}$ direction and has a phase difference between $\hat{x}$ and $\hat{y}$ polarization components. We show that the staggered flux of a minimal plaquette can be tuned freely from 0 to 2π, as required for realizing the CK insulator.

A. Synthetic flux: Previous model

In the previous proposal [30], the s-p_X orbital hybridization is induced by an effective Raman potential $V_R = V_m \cos(\delta\omega t + k_R y)$, where $\delta\omega$ and k_R are the frequency and wave vector of the Raman potential, respectively. The s-p_X orbital hybridization is induced when the frequency difference $\delta\omega$ compensates the energy difference between s and p_X orbitals, and can be calculated through the rotating-wave approximation. To examine the hopping and flux generated by the V_R, we calculate the hopping integrals of a loop round a minimal square [see Fig. 1(a)] and find that the hopping integrals take the following form (details of the calculation can be found in the Appendix):

$$J_1 = \int d^2r\, \psi^p_{n,m}\psi^s_{n+1,m}e^{ik_R y} = e^{ik_R m} I_a,$$
$$J_2 = \int d^2r\, \psi^p_{n+1,m+1}\psi^s_{n+1,m}e^{-ik_R y} = -e^{-ik_R(m+\frac{1}{2})} I^*_b,$$
$$J_3 = \int d^2r\, \psi^p_{n+1,m+1}\psi^s_{n,m+1}e^{ik_R y} = -e^{ik_R(m+1)} I^*_a,$$
$$J_4 = \int d^2r\, \psi^p_{n,m}\psi^s_{n,m+1}e^{-ik_R y} = e^{-ik_R(m+\frac{1}{2})} I_b,$$

where $\psi^p_{n,m}$ ($\psi^s_{n,m}$) denotes real maximally localized Wannier function for s (p_X) orbital localized at the site $(m, n)a'$, with $a' = a/\sqrt{2}$ and a being the lattice constant of sublattice. For simplicity we set the lattice constant $a = 1$. The orbitals $\psi^s_{0,0}(x, y)$ and $\psi^p_{0,0}(x, y)$ are parity even and parity odd, respectively. The quantities I_a and I_b are complex. From the above result it is apparent that the product of four hopping integrals is real, implying zero synthetic magnetic flux over a loop of a plaquette, even though the flux over a triangular $(n, m) \to (n + 1, m) \to (n + 1, m + 1) \to (n, m)$ might be nonzero. Thus, time-reversal symmetry is broken, while we can show that this does not lead to QAH effect. If we apply a gauge transformation $c^\dagger_{s,n,m} \to c^\dagger_{s,n,m}e^{ik_R m}$, in our basis the hopping integrals become

$$J_1 = I_a, \quad J_2 = -e^{\frac{i}{2}k_R} I^*_b,$$
$$J_3 = -I^*_a, \quad J_4 = e^{-i\frac{i}{2}k_R} I_b. \tag{1}$$

From the above results one can easily find that the tight-binding Hamiltonian in k space lacks the τ_x term, and cannot lead to QAH effect.

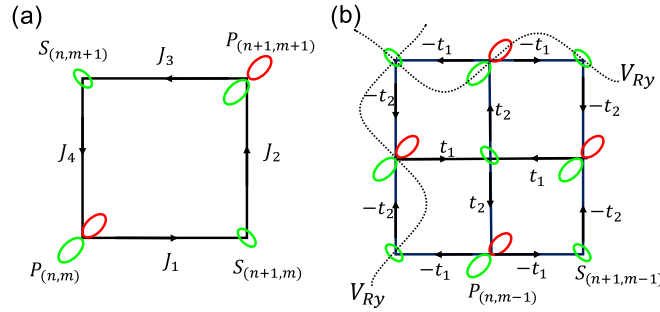

FIG. 1. (a) Laser-induced s-p_X hoppings in previous setup [30] for one plaquette of the double-well optical lattice. (b) Laser-induced s-p_X hybridization in our scheme for four nearest plaquettes of the double-well optical lattice.

B. Improved scheme

Note that the optical lattice potentials for the checkerboard lattice [see Fig. 2(a)] are formed by the following standing

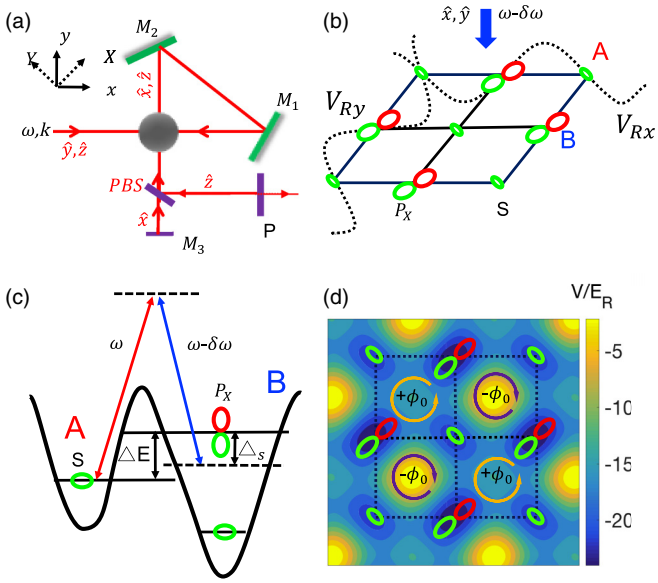

FIG. 2. (a) Sketch of generating double-well checkerboard superlattice by a laser beam proposed in Ref. [30]. (b) The checkerboard sublattice and Raman potential for the improved scheme. (c), (d) The Raman coupling that induces s-p_X orbital hybridization (c) and creates staggered flux pattern displayed in (d), with the lattice potential parameters taken as $(V_0, V_1, V_2) = (8, 8, 5)E_R$ and $\phi_0 = 2\phi$.

wave fields [30]:

$$\mathbf{E}_{xy} = 2E_1[\cos(k_0 x)\hat{y} + \cos(k_0 y)\hat{x}],$$
$$\mathbf{E}_z = E_2[e^{ik_0 x} + e^{ik_0 y} + \alpha e^{-ik_0 x + i\pi} + \alpha e^{ik_0 y + i\pi}]\hat{z}, \quad (2)$$

which induces the optical lattice potential as $V_{\text{latt}} = -V_0[\cos^2(k_0 x) + \cos^2(k_0 y)] - V_1 \sin^2[(k_0/2)(x-y)] - V_2 \sin^2[(k_0/2)(x+y)]$, with the parameter α used to tuning the relative magnitudes of the lattice depths $V_{0,1,2}$.

In the present improved scheme, to generate staggered synthetic magnetic flux, we add an additional incident beam with electric field

$$\tilde{\mathbf{E}}_{xy} = E_m e^{ik_z z - i(\omega-\delta\omega)t}(e^{i\phi_x}\hat{x} + e^{i\phi_y}\hat{y}), \quad (3)$$

which propagates along the z direction and is polarized in the x-y planes. The Raman potential [see Fig. 2(b)] is generated by $\tilde{\mathbf{E}}_{xy}$ together with the optical lattice beam $\mathbf{E}_{xy}$. For the two-dimensional (2D) system, one can set that the 2D plane is located at $z = 0$. The Raman potential takes the form

$$V_R \propto E_1 E_m e^{i\delta\omega t}(\cos k_0 y e^{i\phi_x} + \cos k_0 x e^{i\phi_y} + \text{H.c.}). \quad (4)$$

In the rotating-wave approximation, the effective A-B on-site energy difference becomes $\Delta_s = \Delta E - \delta\omega$, where ΔE is the bare energy difference between p_X and s orbitals, as shown in Fig. 2(c). We now compute the hopping integrals generated by V_R. To illustrate the feature of the hopping integral, we consider four small plaquettes [Fig. 1(b)], and calculate the hopping integrals by

$$\begin{aligned} J_{(n,m)\to(n,m+1)} &= t_a e^{-i\phi_y} + t_b e^{-i\phi_x}, \\ J_{(n,m+1)\to(n-1,m+1)} &= -t_a e^{i\phi_x} - t_b e^{i\phi_y}, \\ J_{(n-1,m+1)\to(n-1,m)} &= -t_a e^{-i\phi_y} - t_b e^{-i\phi_x}, \\ J_{(n-1,m)\to(n,m)} &= t_a e^{i\phi_x} + t_b e^{i\phi_y}. \end{aligned} \quad (5)$$

Here, the coefficients t_a and t_b are real quantities, and are calculated by

$$t_a = \int d^2 r\, \psi^p_{-1,0}(x,y)\psi^s_{0,0}(x,y)\cos(k_0 y),$$
$$t_b = -\int d^2 r\, \psi^p_{-1,0}(x,y)\psi^s_{0,0}(x,y)\cos(k_0 x). \quad (6)$$

To obtain the phases of hopping integrals in Eq. (5), we define

$$t_1 = t_a e^{i\phi_x} + t_b e^{i\phi_y},$$
$$t_2 = t_a e^{-i\phi_y} + t_b e^{-i\phi_x}, \quad (7)$$

as shown in Fig. 1(b). The product of the four hopping integrals in Eq. (5) equals to

$$(t_1 t_2)^2 = \left(t_a^2 e^{i\phi_x - i\phi_y} + t_b^2 e^{i\phi_y - i\phi_x} + 2t_a t_b\right)^2. \quad (8)$$

It can be easily seen that when $\phi_x \neq \phi_y$ and $t_a \neq t_b$, the above product is complex, leading to a nonzero staggered flux across a plaquette as illustrated in Figs. 2(d) and 1(b).

The magnitudes of t_a and t_b can be computed using the maximally localized Wannier functions ψ_p and ψ_s. On the other hand, in this work we shall consider the tight-binding regime, in which case, as a good approximation, the coefficients $t_{a,b}$ can be numerically calculated in the following approximate way. We take a rectangle piece of lattice potential containing a single s-p_X double well and solve the orbital wave functions, which replace the Wannier functions in computing $t_{a,b}$. With the parameter condition that $(V_0, V_1, V_2) = (8, 8, 5)E_R$ [30], where $E_R = \hbar^2 k_0^2/(2m)$ is the recoil energy, we find $t_a \approx -2t_b$. Now, the phase ϕ_0 of a plaquette in Eq. (8) can be simplified to

$$\phi_0 = 2\phi = 2\arctan\frac{3\sin(\phi_x - \phi_y)}{5\cos(\phi_x - \phi_y) + 4}, \quad (9)$$

so the total flux ϕ_0 of a plaquette can be tuned from $-\pi$ to π through tuning the phase difference $\phi_x - \phi_y$.

From the relative configuration of lattice and Raman coupling potentials [Fig. 1(b)], we can verify easily that $J_{(n-1,m)\to(n,m)} = -J_{(n,m)\to(n+1,m)}$. For simplicity, we perform the gauge transformation

$$s^\dagger_{m,n,\sigma} \to (-1)^m s^\dagger_{m,n,\sigma},$$
$$p^\dagger_{m,n,\sigma} \to e^{-i\phi_1} p^\dagger_{m,n,\sigma}, \quad (10)$$

where ϕ_1 is the phase of hopping integral t_1 determined through Eq. (7). With above gauge transformation the hopping integrals for s orbitals reverses sign $t_s \to -t_s$, and the phase of s-p_X hopping integral t_1 along $\hat{x}$ direction is transferred to the hopping integral t_2 along $\hat{y}$ direction so that $\pm t_1 \to t_{sp}$ and $\pm t_2 \to t_{sp}e^{i\phi}$. Finally, the tight-binding Hamiltonian

$H = H_0 + H_{\rm int}$ reads as

$$H_0 = \sum_{i\sigma}\left[t_s^Y s_{i\sigma}^\dagger s_{i\pm\hat{Y}\sigma} - \Delta_s s_{i\sigma}^\dagger s_{i\sigma} + t_p^X p_{Xi\sigma}^\dagger p_{Xi\pm\hat{X}\sigma}\right] + \sum_{\langle ij\rangle\sigma} F(\mathbf{r}) s_{i\sigma}^\dagger p_{Xj\sigma}\delta_{j,i+\mathbf{r}} + \text{H.c.}, \tag{11}$$

$$H_{\rm int} = U_s \sum_i \hat{n}_{si\uparrow}\hat{n}_{si\downarrow}, \tag{12}$$

where $s_{j\sigma}^\dagger/p_{Xj\sigma}^\dagger$ are creation operators for s/p_X orbitals at the jth site, $\sigma = \uparrow, \downarrow$, $F(\mathbf{r}) = t_{sp}$ for $\mathbf{r} = \pm\hat{x}$ and $F(\mathbf{r}) = t_{sp}e^{-i\phi}$ for $\mathbf{r} = \pm\hat{y}$ after gauge transformation (10). The interaction part is tuned by Feshbach resonance [30] and we only study the strong repulsive U_s limit. For convenience, we rotate the $\hat{x}$-$\hat{y}$ coordinate frame by 90° to $\hat{X}$-$\hat{Y}$ coordinate frame where $\hat{X} = \hat{x} + \hat{y}$, $\hat{Y} = -\hat{x} + \hat{y}$ when we Fourier transform the tight-binding Hamiltonian. We will use this coordinate frame in the remaining parts. In the $\mathbf{k}$ space, the s and p_X orbitals have dispersion relation $\epsilon_{s\mathbf{k}} = 2t_s^Y \cos k_Y$ and $\epsilon_{p\mathbf{k}} = 2t_p^X \cos k_X$, respectively. The single-particle part of the tight-binding Hamiltonian is written as $H_0 = \sum_{\mathbf{k}\sigma} \mathcal{C}_{\mathbf{k}\sigma}^\dagger \mathcal{H}_0(\mathbf{k})\mathcal{C}_{\mathbf{k}\sigma}$ with $\mathcal{C}_{\mathbf{k}\sigma}^\dagger = (s_{\mathbf{k}\sigma}^\dagger, p_{X\mathbf{k}\sigma}^\dagger)$ and the Bloch Hamiltonian takes the form

$$\mathcal{H}_0(\mathbf{k}) = d_0(\mathbf{k})\tau_0 + d_x(\mathbf{k})\tau_x + d_y(\mathbf{k})\tau_y + d_z(\mathbf{k})\tau_z, \tag{13}$$

where $d_x(\mathbf{k}) = 2t_{sp}(\cos\phi\cos\frac{k_X+k_Y}{2} + \cos\frac{k_X-k_Y}{2})$, $d_y(\mathbf{k}) = 2t_{sp}\sin\phi\cos\frac{k_X+k_Y}{2}$, $d_{0/z}(\mathbf{k}) = \pm t_p^X\cos k_X + t_s^Y\cos k_Y - \Delta_s/2$, and the Pauli matrix $\tau_{x,y,z}$ act on orbital space. The single-particle Hamiltonian H_0 leads to a QAH phase when $|\Delta_s| < 2(t_s + t_p)$ and $0 < \phi < \pi$ [30].

III. RKKY MAGNETIC INTERACTION

The RKKY interaction in Kondo lattice systems usually refers to the indirect coupling between local moments induced by the hybridization between local f electrons and itinerant d electrons in solid-state physics. The competition between RKKY interaction (characterized by the Néel temperature $|J_K\rho|^2$) and Kondo effect [characterized by the Kondo temperature $T_K \sim \exp(-1/|J_K\rho|)$] is described by the Doniach diagram [61] which states that the RKKY interaction dominates in the weak $|J_K|$ limit and the Kondo effect dominates in the large $|J_K|$ limit. To investigate the possible magnetic phases in our CK model, we derive the effective RKKY interaction in this section through two steps. We first derive the effective Kondo lattice Hamiltonian from our CK model in Sec. III A, and then derive the effective RKKY interaction in Sec. III B based on the Kondo lattice Hamiltonian obtained in Sec. III A. We also analyze the static magnetic susceptibility of the RKKY interaction in Sec. III B. The static susceptibility is affected by the Fermi surface nesting effect and the ϕ-dependent hybridization. We will show that the Fermi surface nesting effect of the p_X band always favors staggered magnetic order in the $\hat{X}$ direction, while the hybridization may favor different magnetic orders for different phase ϕ of the s-p_X hybridization.

A. Effective Kondo lattice Hamiltonian

The Kondo lattice Hamiltonian is the effective Hamiltonian derived from the periodic Anderson model by eliminating valence fluctuations and performing second-order perturbation in the Kondo regime where the hybridization is weak and the local orbital onsite energy lies far below the Fermi level of itinerant band. This step can be done either by Schrieffer-Wolff transformation [67] or by projection operator [68]. In this paper, we take the latter method to handle our CK model, which is also convenient for deriving the RKKY interaction.

We perform the perturbation in the $t_s^Y = 0$ and $U_s = +\infty$ limit. The Hamiltonian $H = H_1 + H'$ is separated into two parts: H_1 preserves occupancy number of s orbital atoms, and the hybridization term H' mixes the subspaces with different number of s-orbital atoms:

$$H_1 = \sum_{i\sigma}\left[-\Delta_s s_{i\sigma}^\dagger s_{i\sigma} + t_p^X p_{Xi\sigma}^\dagger p_{Xi\pm\hat{X}\sigma}\right] + \sum_i U_s \hat{n}_{si\uparrow}\hat{n}_{si\downarrow},$$

$$H' = \sum_{\mathbf{k},i}\frac{V_{\mathbf{k}}e^{-i\mathbf{k}\cdot\mathbf{R}_i}}{\sqrt{N}} s_{i\sigma}^\dagger p_{Xk\sigma} + \text{H.c.}, \tag{14}$$

where $V_{\mathbf{k}} = 2t_{sp}[\exp(i\phi)\cos\frac{k_X+k_Y}{2} + \cos\frac{k_X-k_Y}{2}]$ is the hybridization function in $\mathbf{k}$ space, N denotes the number of unit cells, and $\mathbf{R}_i$ denotes the s-orbital position in the $\hat{X}$-$\hat{Y}$ coordinate frame. The H' term is treated as a perturbation if the hybridization strength is weak. Experimentally, the magnitude of t_{sp} can be tuned independently of the optical lattice by the strength of the Raman laser. To obtain the effective Hamiltonian, we define projection operator P and $Q = 1 - P$, where P projects onto the subspace in which each s orbital is singly occupied. From the Schrödinger equation, we obtain the following equations:

$$\begin{aligned}(P+Q)H(P+Q)\psi &= E\psi,\\ PH(P+Q)\psi &= EP\psi,\\ QH(P+Q)\psi &= EQ\psi.\end{aligned} \tag{15}$$

We eliminate $Q\psi$ to obtain effective Hamiltonian in subspace P:

$$H_p(E) = PHP - PHQ\frac{1}{QHQ - E}QHP, \tag{16}$$

where $H_p(E)$ is the effective Hamiltonian that satisfies

$$H_p(E)[P\psi] = E[P\psi]. \tag{17}$$

The approximation we then consider is to substitute the unknown eigenenergy E by the energy of the unperturbed states E_0. The product of operators PHQ and QHP only keeps second-order virtual processes that the states in subspace P transfer to subspace Q and then return back to subspace P. After some algebra (see the Appendix for details) we obtain the effective Kondo lattice Hamiltonian:

$$H_{\rm KL} = \sum_{\mathbf{k}\sigma}\epsilon_{p\mathbf{k}}p_{X\mathbf{k}\sigma}^\dagger p_{X\mathbf{k}\sigma} + \sum_{i,\mathbf{k},\mathbf{k}'} 2J_{\mathbf{k},\mathbf{k}',i}\mathbf{S}_i\cdot\mathbf{s}_{\mathbf{k}\mathbf{k}'}, \tag{18}$$

where we have defined the s-orbital spin operators $\mathbf{S}_i = s_{i\sigma'}^\dagger\boldsymbol{\tau}_{\sigma'\sigma}s_{i\sigma}/2$, p_X-orbital spin operators $\mathbf{s}_{\mathbf{k},\mathbf{k}'} = p_{X\mathbf{k}\sigma'}^\dagger\boldsymbol{\tau}_{\sigma'\sigma}p_{X\mathbf{k}'\sigma}/2$, and the anistropic $\mathbf{k}$-dependent Kondo

coupling $J_{\mathbf{k},\mathbf{k}',i} = \frac{1}{N}\frac{V_{\mathbf{k}}^* V_{\mathbf{k}'} e^{i(\mathbf{k}-\mathbf{k}')\cdot R_i}}{\epsilon_{p\mathbf{k}}+\Delta_s}$, which contains the information of the hybridization between s and p_X orbitals.

B. RKKY interaction and static spin susceptibility

The RKKY interaction is derived from the Kondo lattice model in weak Kondo coupling J regime by second-order perturbation at the cost of eliminating the itinerant electron degree of freedom. Although the Kondo effect is omitted in such perturbation treatment, the RKKY interaction is helpful for searching possible magnetic orders. We now derive the RKKY interaction based on the Kondo lattice model obtained in the last subsection by applying the projection operator method again. In the perturbation treatment, it is assumed that the p_X band is treated as free band without coupling to the s orbitals, while the s-p_X hybridization shall be considered up to second order to derive RKKY interaction for s orbitals. Thus, the p_X orbital has the Fermi level ϵ_{p,k_F}. The p_X orbital states have fermion distribution $n_{p,k} = 1$ if $\epsilon_{p,k} < \epsilon_{p,k_F}$, and $n_{p,k} = 0$ if $\epsilon_{p,k} > \epsilon_{p,k_F}$. We further define that the projection operator P_0 projects states onto the subspace with a ground-state Fermi sea formed by the p_X-orbital degree of freedom, so in subspace P_0 no particle excitation above Fermi sea or hole excitation below Fermi sea exists. By the second-order perturbation (see details in the Appendix) similar to that in the above subsection, we obtain the RKKY interaction

$$H_{\mathrm{RKKY}} = \sum_{i,j} 2J(X_i - X_j, Y_i - Y_j)\mathbf{S}_i \cdot \mathbf{S}_j, \tag{19}$$

where the coupling coefficient takes the form

$$\begin{aligned} &J(X_i - X_j, Y_i - Y_j) \\ &= \sum_{\mathbf{k},\mathbf{k}'} \frac{4\cos[(\mathbf{k}-\mathbf{k}')\cdot(\mathbf{R}_i - \mathbf{R}_j)]}{N^2} \\ &\quad \times |V_{\mathbf{k}}|^2 |V_{\mathbf{k}'}|^2 \frac{1}{\epsilon_{p\mathbf{k}}+\Delta_s}\frac{1}{\epsilon_{p\mathbf{k}'}+\Delta_s}\frac{n_{p,\mathbf{k}} - n_{p,\mathbf{k}'}}{\epsilon_{p\mathbf{k}} - \epsilon_{p\mathbf{k}'}}. \end{aligned} \tag{20}$$

The static spin susceptibility $\chi(\mathbf{Q})$, which is the Fourier transformation of the real-space coupling coefficient $J(X_i - X_j, Y_i - Y_j)$, can then be obtained directly:

$$\begin{aligned} \chi(\mathbf{Q}) = \sum_{\mathbf{k}} 2|V_{\mathbf{k}}|^2 |V_{\mathbf{k}+\mathbf{Q}}|^2 \frac{1}{\epsilon_{p,\mathbf{k}}+\Delta_s}\frac{1}{\epsilon_{p,\mathbf{k}+\mathbf{Q}}+\Delta_s} \\ \times \frac{n_{p,\mathbf{k}} - n_{p,\mathbf{k}+\mathbf{Q}}}{\epsilon_{p,\mathbf{k}} - \epsilon_{p,\mathbf{k}+\mathbf{Q}}}. \end{aligned} \tag{21}$$

The $\chi(\mathbf{Q})$ is just the dispersion relation of the RKKY interaction Hamiltonian [69] if we view the quantum spin model (19) as a classical spin model, and the vector Q which minimizes $\chi(\mathbf{Q})$ is the ground-state magnetic order of the corresponding classical spin model.

From Eq. (21) one can find the susceptibility function of Q is different from that in a standard Kondo lattice model. On one hand, the hybridization function $|V_{\mathbf{k}}|^2 = 4t_{sp}^2\{\cos\phi[\cos(k_X) + \cos(k_Y)] + \cos(k_X)\cos(k_Y) + 1\}$ is $\mathbf{k}$ and ϕ dependent, originating from the feature of the superlattice that each p_X orbital resides in the center of four nearest-neighbor s orbitals and can hop directly to one of them with phase. On the other hand, the dispersion of the itinerant p_X band is highly anisotropic and relevant only in one dimension, while the model is two dimensional due to the two-dimensional hybridization. For simplicity we replace the term $1/(\epsilon_{p,\mathbf{k}} + \Delta_s)$ with $1/(\epsilon_{p,\mathbf{k}_F} + \Delta_s)$ since the particle scattering mostly occurs near the Fermi level $\epsilon_{p,\mathbf{k}_F}$. We can then find the RKKY interaction with ϕ is equivalent to that with π-ϕ and the magnetic phase diagram from this approach is symmetric about $\phi = \pi/2$.

To see clearly the magnetic effects from the susceptibility equation (21), we separately look at the contributions from the Fermi surface nesting term

$$\sum_{\mathbf{k}} \frac{n_{p,\mathbf{k}} - n_{p,\mathbf{k}+\mathbf{Q}}}{\epsilon_{p,\mathbf{k}} - \epsilon_{p,\mathbf{k}+\mathbf{Q}}}, \tag{22}$$

and from the hybridization term

$$\begin{aligned} \sum_{\mathbf{k}} |V_{\mathbf{k}}|^2 |V_{\mathbf{k}+\mathbf{Q}}|^2 &\propto -\cos Q_X \cos Q_Y \\ &\quad - 2\cos\phi^2(\cos Q_X + \cos Q_Y) - 4. \end{aligned} \tag{23}$$

It can be seen that the Fermi surface nesting term (22) tends to result in antiferromagnetic order (AF) with $Q_X = 2k_F = \pi$ in the $\hat{X}$ direction since the p_X orbitals only hop in the $\hat{X}$ direction and the band formed by p_X orbitals is half-filled. On the other hand, the effect of the hybridization term (23) depends on the phase ϕ. For $\phi = \pi/2$, Eq. (23) equals to $-\cos Q_X \cos Q_Y - 4$ and favors the magnetic order with $\mathbf{Q} = (0,0)$ or (π,π); while for $\phi = 0$ or π, Eq. (23) equals to $-(\cos Q_X + 2)(\cos Q_Y + 2)$ and favors the magnetic order with $\mathbf{Q} = (0,0)$. The order $\mathbf{Q} = (0,0)$ therefore competes with the Fermi surface nesting effect in the $\hat{X}$ direction. We numerically calculated Eq. (21) and plotted the one-dimensional magnetic phase diagram in Fig. 3. The figure shows that near $\phi = \pi/2$ the order is AF with $\mathbf{Q} = (\pi,\pi)$ while near $\phi = 0$ or π the order is collinear antiferromagnetic order (CAF) with $\mathbf{Q} = (\pi, 0)$, implying that the Fermi surface nesting effect dominates in weak hybridization regime. We

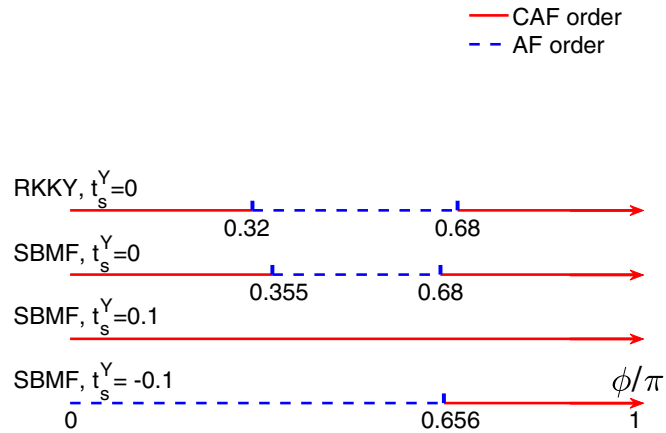

FIG. 3. One-dimensional magnetic phase diagrams with $(t_p^X, t_{sp}, \Delta_s) = (1, 0.3, 3)$ determined by phase ϕ. The phase diagram on the top is obtained from RKKY interaction by perturbation theory with $t_s^Y = 0$, and three lower phase diagrams are obtained with slave-boson mean-field theory (SBMF) with different t_s^Y. The red solid lines correspond to CAF order with $Q = (\pi, 0)$ and blue dashed lines correspond to AF order with $Q = (\pi, \pi)$.

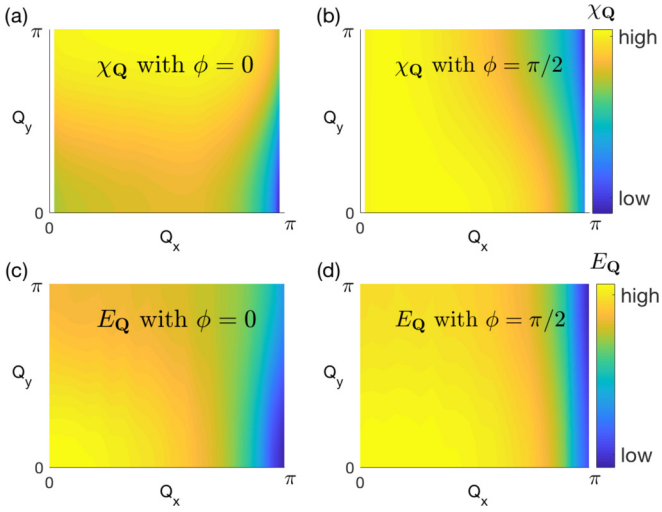

FIG. 4. Magnetic susceptibility/slave-boson mean-field energy as functions of magnetic order $\mathbf{Q}$ with $(t_s^Y, t_p^X, t_{sp}, \Delta_s) = (0, 1, 0.5, 3)$ for $\phi = 0$ and $\pi/2$. The dark blue and yellow colors represent the minimum and maximum of the susceptibility/energy, respectively. (a), (b) Static susceptibility $\chi_{\mathbf{Q}}$ obtained from RKKY interaction by perturbation theory for $\phi = 0$ and $\pi/2$. In the limit $Q_X = \pi$ the susceptibility diverges. (c), (d) Mean-field energy $E_{\mathbf{Q}}$ obtained with slave-boson mean-field theory for $\phi = 0$ and $\pi/2$. For (a) and (c), the ground-state magnetic order is $(\pi, 0)$; for (b) and (d), the ground-state magnetic order is (π, π).

also plotted a special case of Eq. (21) with $(t_s^Y, t_p^X, t_{sp}, \Delta_s) = (0.1, 1, 0.5, 3)$ as a function of Q_X and Q_Y in Figs. 4(a) and 4(b). Note that at $Q_X = \pi$ in Eq. (22) and the susceptibility diverges due to the one-dimensional character of p_X band dispersion, although the magnetic order is two dimensional due to the two-dimensional hybridization.

We further investigate the properties of RKKY interaction in real space from Eq. (19). In the $\hat{Y}$ direction, coupling coefficients with $|Y_i - Y_j| > 1$ always vanish due to the anisotropic p_X band and the RKKY magnetic interaction is the fourth-order virtual process with respect to t_{sp}. While in the $\hat{X}$ direction, as the value of Eq. (22) diverges at $Q_X = \pi$ due to one-dimensional character of $\epsilon_{p\mathbf{k}}$, the coupling coefficients decay slowly. As a result, the coupling coefficients are short ranged in the $\hat{Y}$ direction and long ranged in the $\hat{X}$ direction. We numerically calculated the coupling coefficients $J(X_i - X_j, Y_i - Y_j)$ with Eq. (19) for $\phi = \pi/2$ and 0 as shown in

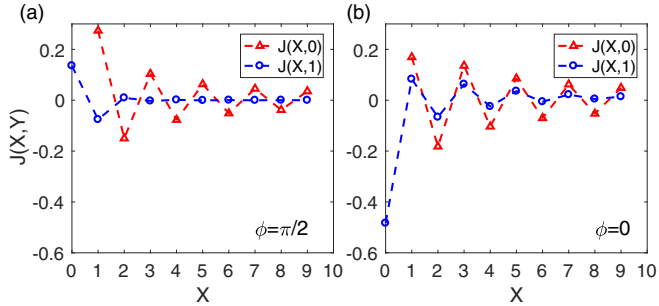

FIG. 5. The RKKY coupling coefficient $J(X, Y) = J(X_i - X_j, Y_i - Y_j)$ with $(t_s^Y, t_p^X, \Delta_s) = (0, 1, 3)$ for (a) $\phi = \pi/2$ and (b) $\phi = 0$ in the unit of $|J(0, 0)|$.

Fig. 5. The signs of $J(X, 0)$ in the two cases are the same and favor $Q_X = \pi$ order. However, the signs of $J(X, 1)$ in the two cases differ by -1, and it can be seen that $Q_Y = \pi$ is supported when $\phi = \pi/2$ while $Q_Y = 0$ is supported when $\phi = 0$, which is consistent with Fig. 3. As the signs of $J(X, Y)$ oscillate, there is no geometric frustration in these two special cases. From these results, we obtain that when ϕ is tuned from 0 to $\pi/2$ or from π to $\pi/2$, the magnetism has a transition from CAF order to AF order, as shown in Fig. 3.

IV. MAGNETIC PHASES AND THEIR EFFECTS ON QAH KONDO STATES

Note that the RKKY interaction, which shows the possible magnetic orders, is obtained by perturbation theory and valid in weak hybridization regime. Moreover, the derivation of the effective RKKY interaction is at the cost of eliminating the p_X orbital degree of freedom, which fails to study Kondo and QAH effects since only the s orbital is left. To overcome these drawbacks, in this section we apply the nonperturbative slave-boson mean-field theory to study the ground-state phases and magnetic effects on the QAH effect in our CK model. To take into account the magnetic orders suggested by the RKKY interaction, we apply the spin-rotation invariant slave-boson mean-field theory [73] in Sec. IV A, which is convenient to describe various magnetic orders. In Secs. IV B and IV C, we show the magnetic and correlated QAH phase diagrams in Fig. 6, and in Sec. IV D we discuss how to identify the influences of strong correlation and magnetism on the CK phase by measuring Hall conductance and double occupancy in cold atom experiments. Different from the previous work [30], we show the rich magnetic phases coexisting with Kondo hybridization and find that in the magnetic Kondo phases the effective hybridization, and then the correlated QAH phase, are enhanced compared with the paramagnetic Kondo phase in relatively weak hybridization regime.

A. Slave-boson mean-field theory

In the present CK model (periodic Anderson model), due to the strong repulsive Hubbard interaction in s orbitals, the double occupancy of s orbitals is suppressed to zero. Such a system can be studied with slave-boson theory [70] proposed by Coleman. Kotliar and Ruckenstein (KR) further extended the Coleman slave-boson representation to a more complex form [71] that incorporates the result of the Gutzwiller approximation [72] on the mean-field level. In this paper, we apply the spin-rotation invariant slave-boson mean-field theory [73] which is a generalized form of the KR slave-boson theory and is convenient to explore various magnetic orders.

In the spin-rotation invariant slave-boson theory [73], the auxiliary bosonic and fermionic operators can be introduced. For this we introduce the slave-boson operators $\hat{e}$, $\hat{d}$, $\hat{p}_0$, $\hat{\mathbf{p}} = (\hat{p}_1, \hat{p}_2, \hat{p}_3)$ that obey bosonic commutation relation. Here, $\hat{e}$, $\hat{d}$ correspond to hole and doubly occupied states. The scalar $(S = 0)$ field $\hat{p}_0$ and vector $(S = 1)$ field $\hat{\mathbf{p}} = (\hat{p}_1, \hat{p}_2, \hat{p}_3)$ correspond to the singly occupied state. Note that $\hat{e}$, $\hat{d}$, $\hat{p}_0$ transform as scalars under spin rotation, while $\hat{\mathbf{p}}$ transforms as a vector. On the other hand, the $S = \frac{1}{2}$ pseudofermion operators $c_{i\sigma}$ obey fermionic commutation relation. The key idea

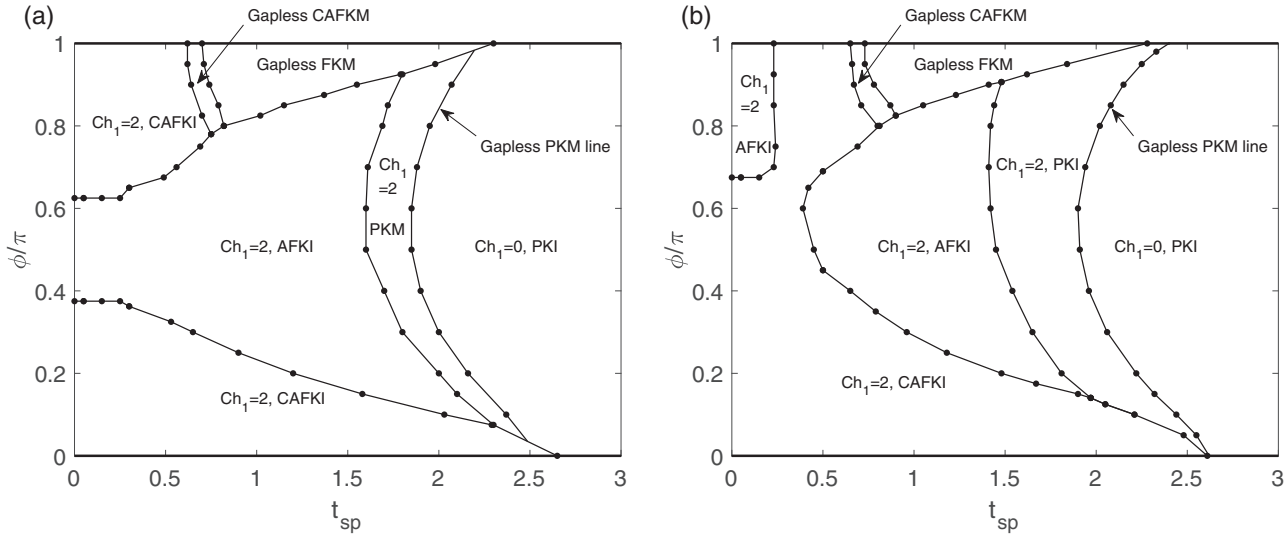

FIG. 6. The magnetic and QAH phase diagrams based on slave-boson theory for $(t_p^X, \Delta_s) = (1, 3)$ for $t_s^Y = 0$ in (a) and $t_s^Y = 0.1$ in (b), respectively. The Ch_1 refers to as the first Chern number. The phases shown here include antiferromagnetic Kondo insulator (AFKI), collinear antiferromagnetic Kondo insulator (CAFKI), collinear antiferromagnetic Kondo metal (CAFKM), ferromagnetic Kondo metal (FKM), paramagnetic Kondo insulator (PKI), and paramagnetic Kondo metal (PKM) phases. The dotted lines represent phase boundaries. The Chern number for $\phi = 0$ and π lines is always zero but is not displayed in the figure.

is that the singly occupied auxiliary bosonic and fermionic modes shall form into spin-$\frac{1}{2}$ s-orbtial fermion states under proper constraints. The local s-orbital operators s_σ are then represented by $s_\sigma = \sum_{\sigma'} \hat{z}_{\sigma\sigma'} c_{\sigma'}$, with the matrix $\underline{z}$ defined as (see more details in the Appendix)

$$\underline{\hat{z}} = \hat{e}^\dagger \underline{L} \underline{R} \underline{\hat{p}} + \underline{\hat{\tilde{p}}}^\dagger \underline{L} \underline{R} \hat{d}, \tag{24}$$

where

$$\underline{L} = [(1 - \hat{d}^\dagger \hat{d})\underline{1} - 2\underline{\hat{p}}^\dagger \underline{\hat{p}}]^{-\frac{1}{2}},$$
$$\underline{R} = [(1 - \hat{e}^\dagger \hat{e})\underline{1} - 2\underline{\hat{\tilde{p}}}^\dagger \underline{\hat{p}}]^{-\frac{1}{2}}. \tag{25}$$

Here, $\underline{\hat{z}}, \underline{L}, \underline{R}$ are 2×2 matrices, matrix elements of the matrix $\underline{\hat{p}}$ are defined as $\hat{p}_{\sigma\sigma'} = \frac{1}{2} \sum_{\mu=0}^{3} \hat{p}_\mu \tau_{\mu,\sigma\sigma'}$, and its time-reversal transformation reads as $\hat{\tilde{p}}_{\sigma\sigma'} = (\hat{T} \underline{\hat{p}} \hat{T}^{-1})_{\sigma\sigma'} = \sigma\sigma' \hat{p}_{\bar{\sigma}'\bar{\sigma}}$. For each s orbital at site $\mathbf{R}_i$, a set of above auxiliary operators are induced with index i labeling their sites. The total Hilbert space has been extended now and the physical subspace can be obtained through the following constraints:

$$\hat{e}_i^\dagger \hat{e}_i + \hat{d}_i^\dagger \hat{d}_i + \sum_\mu \hat{p}_{i\mu}^\dagger \hat{p}_{i\mu} - 1 = 0,$$
$$\sum_\sigma c_{i\sigma}^\dagger c_{i\sigma} - \sum_\mu \hat{p}_{i\mu}^\dagger \hat{p}_{i\mu} - 2\hat{d}_i^\dagger \hat{d}_i = 0, \tag{26}$$
$$\sum_{\sigma\sigma'} \boldsymbol{\tau}_{\sigma\sigma'} c_{i\sigma'}^\dagger c_{i\sigma} - \hat{p}_{i0} \hat{\mathbf{p}}_i^\dagger - \hat{\mathbf{p}}_i^\dagger \hat{p}_{i0} + i(\hat{\mathbf{p}}_i^\dagger \times \hat{\mathbf{p}}_i) = 0.$$

In terms of the auxiliary operators and incorporating the constraints in the form of Lagrange multiplier fields α_i, β_{i0}, and $\boldsymbol{\beta}_i$, the CK Hamiltonian takes the form

$$H = \sum_{i\sigma} \left[\sum_{\sigma'\sigma''} t_s^Y \hat{z}_{i\sigma\sigma'}^\dagger \hat{z}_{i\pm\hat{Y}\sigma''\sigma} c_{i\sigma'}^\dagger c_{i\pm\hat{Y}\sigma''} - \Delta_s c_{i\sigma}^\dagger c_{i\sigma} + t_p^X p_{Xi\sigma}^\dagger p_{Xi\pm\hat{X}\sigma} \right] + \left[\sum_{\langle ij \rangle \sigma} F(\mathbf{r}) \hat{z}_{i\sigma\sigma'}^\dagger c_{i\sigma'}^\dagger p_{Xj\sigma} \delta_{j,i+\mathbf{r}} + \mathrm{H.c.} \right]$$
$$+ \sum_i \left[U_s \hat{d}_i^\dagger \hat{d}_i + \alpha_i \left(\hat{e}_i^\dagger \hat{e}_i + \hat{d}_i^\dagger \hat{d}_i + \sum_\mu \hat{p}_{i\mu}^\dagger \hat{p}_{i\mu} - 1 \right) + \beta_{i0} \left(\sum_\sigma c_{i\sigma}^\dagger c_{i\sigma} - \sum_\mu \hat{p}_{i\mu}^\dagger \hat{p}_{i\mu} - 2\hat{d}_i^\dagger \hat{d}_i \right) \right.$$
$$\left. + \boldsymbol{\beta}_i \cdot \left(\sum_{\sigma\sigma'} \boldsymbol{\tau}_{\sigma\sigma'} c_{i\sigma'}^\dagger c_{i\sigma} - \hat{p}_{i0} \hat{\mathbf{p}}_i^\dagger - \hat{\mathbf{p}}_i^\dagger \hat{p}_{i0} + i(\hat{\mathbf{p}}_i^\dagger \times \hat{\mathbf{p}}_i) \right) \right]. \tag{27}$$

We consider the mean-field approximation to the boson fields in the above Hamiltonian with infinitely large s-orbital onsite interaction U_s. In this case, the scalar bosonic mean-field order vanishes $d_i = 0$, the scalar mean-field orders e_i, p_{0i} can be assumed spatially uniform so that $e_i = e$ and $p_{0i} = p_0$, and also the Lagrange multiplier fields $\alpha_i = \alpha$, $\beta_{0i} = \beta_0$. We further consider that the vector mean-field orders take the forms $\mathbf{p}_i = p(\cos(\mathbf{Q} \cdot \mathbf{R}_i), \sin(\mathbf{Q} \cdot \mathbf{R}_i), 0)$ and

$\boldsymbol{\beta}_i = \beta(\cos(\mathbf{Q}\cdot\mathbf{R}_i), \sin(\mathbf{Q}\cdot\mathbf{R}_i), 0)$, characterizing a spatially rotation structure in the $\hat{X}$-$\hat{Y}$ plane. The magnetic order wave vector $\mathbf{Q}$ can be commensurate or incommensurate. In particular, $\mathbf{Q} = (\pi, \pi)$ denotes AF order, while the order is incommensurate if any component of $\mathbf{Q}/\pi$ is irrational. Based on the above assumptions, the mean-field Hamiltonian (see details in the Appendix) in the basis $\mathbf{X}_\mathbf{k}^\dagger \equiv (c_{\mathbf{k}\uparrow}^\dagger, c_{\mathbf{k}+\mathbf{Q}\downarrow}^\dagger, p_{X\mathbf{k}\uparrow}^\dagger, p_{X\mathbf{k}+\mathbf{Q}\downarrow}^\dagger)$ takes the form

$$H = \sum_k \mathbf{X}_\mathbf{k}^\dagger \epsilon_k \mathbf{X}_\mathbf{k} + N\big[-\beta_0\big(p_0^2 + p^2\big) + 2\beta p_0 p + \alpha\big(e^2 + p^2 + p_0^2 - 1\big)\big], \tag{28}$$

with matrix ϵ_k defined as

$$\epsilon_k = \begin{pmatrix} \epsilon_{s\mathbf{k}}^a + \beta_0 & \epsilon_{s\mathbf{k}}^c + \beta & z_+ V_\mathbf{k} & z_- V_{\mathbf{k}+\mathbf{Q}} \\ \epsilon_{s\mathbf{k}}^c + \beta & \epsilon_{s\mathbf{k}}^b + \beta_0 & z_- V_\mathbf{k} & z_+ V_{\mathbf{k}+\mathbf{Q}} \\ z_+ V_\mathbf{k}^* & z_- V_\mathbf{k}^* & \epsilon_{p,\mathbf{k}} & 0 \\ z_- V_{\mathbf{k}+\mathbf{Q}}^* & z_+ V_{\mathbf{k}+\mathbf{Q}}^* & 0 & \epsilon_{p,\mathbf{k}+\mathbf{Q}} \end{pmatrix}. \tag{29}$$

Here, $\epsilon_{s\mathbf{k}}^a = z_+^2 \epsilon_{s\mathbf{k}} + z_-^2 \epsilon_{s\mathbf{k}+\mathbf{Q}} - \Delta_s$, $\epsilon_{s\mathbf{k}}^b = z_+^2 \epsilon_{s\mathbf{k}+\mathbf{Q}} + z_-^2 \epsilon_{s\mathbf{k}} - \Delta_s$, $\epsilon_{s\mathbf{k}}^c = z_+ z_- (\epsilon_{s\mathbf{k}+\mathbf{Q}} + \epsilon_{s\mathbf{k}})$ are s-orbital hopping terms. The renormalization factor takes the form [74]

$$z_\pm = \frac{1}{\sqrt{2}} \frac{ep_+}{\sqrt{1-p_+^2}\sqrt{1-e^2-p_-^2}} \pm \frac{1}{\sqrt{2}} \frac{ep_-}{\sqrt{1-p_-^2}\sqrt{1-e^2-p_+^2}}, \tag{30}$$

where $p_\pm = (p_0 \pm p)/\sqrt{2}$ are proportional to the eigenvalues of the $\hat{p}_{\sigma\sigma'}$ matrix.

The mean-field solutions (saddle-point approximation) are obtained by minimizing the mean-field free energy (ground-state energy at zero temperature), which reads as

$$F = -T\sum_{\mathbf{k}\alpha} \ln[1 + \exp[-(E_{\mathbf{k}\alpha} - \mu)/T]] + N\big[-\beta_0\big(p_0^2 + p^2\big) + 2\beta p_0 p + \alpha\big(e^2 + p^2 + p_0^2 - 1\big)\big]. \tag{31}$$

Here, the $\epsilon_{\mathbf{k}\alpha}$ with $\alpha = 1, 2, 3, 4$ are four eigenvalues of the 4×4 matrix $\epsilon_\mathbf{k}$. The stationary condition yields the saddle-point equations

$$\frac{\partial F}{\partial e} = \frac{\partial F}{\partial p_0} = \frac{\partial F}{\partial p} = \frac{\partial F}{\partial \alpha} = \frac{\partial F}{\partial \beta_0} = \frac{\partial F}{\partial \beta} = 0. \tag{32}$$

The chemical potential μ at half-filling is determined by the particle-number condition

$$\sum_{\mathbf{k}\alpha} f(E_{\mathbf{k}\alpha} - \mu) = 2N, \tag{33}$$

where f is the Fermi-Dirac distribution function. Since we only consider the ground state in this paper, the distribution function is just a step function.

The physical quantities such as particle numbers and magnetic moments can be represented by correlation functions. Particle number and magnetic moment in s orbitals are obtained by

$$\begin{aligned} n_{s\uparrow} &= \sum_{\mathbf{k}\in BZ} \langle c_{\mathbf{k}\uparrow}^\dagger c_{\mathbf{k}\uparrow}\rangle, \\ n_{s\downarrow} &= \sum_{\mathbf{k}\in BZ} \langle c_{\mathbf{k}\downarrow}^\dagger c_{\mathbf{k}\downarrow}\rangle, \\ \mathbf{m}_s &= \sum_{\mathbf{k}\in BZ,\sigma\sigma'} \langle c_{\mathbf{k}\sigma}^\dagger \boldsymbol{\tau}_{\sigma\sigma'} c_{\mathbf{k}+\mathbf{Q}\sigma'}\rangle. \end{aligned} \tag{34}$$

Similarly, the particle number and magnetic moment in p_X orbitals take the form

$$\begin{aligned} n_{p\uparrow} &= \sum_{\mathbf{k}\in BZ} \langle p_{X\mathbf{k}\uparrow}^\dagger p_{X\mathbf{k}\uparrow}\rangle, \\ n_{p\downarrow} &= \sum_{\mathbf{k}\in BZ} \langle p_{X\mathbf{k}\downarrow}^\dagger p_{X\mathbf{k}\downarrow}\rangle, \\ \mathbf{m}_p &= \sum_{\mathbf{k}\in BZ,\sigma\sigma'} \langle p_{X\mathbf{k}\sigma}^\dagger \boldsymbol{\tau}_{\sigma\sigma'} p_{X\mathbf{k}+\mathbf{Q}\sigma'}\rangle. \end{aligned} \tag{35}$$

The first Chern number Ch_1 for the bands below Fermi level μ is calculated by

$$\mathrm{Ch}_1 = \int_{BZ} d^2\mathbf{k} \sum_{\alpha,\alpha'} [f(E_{\mathbf{k}\alpha'} - \mu) - f(E_{\mathbf{k}\alpha} - \mu)] \times \frac{1}{2\pi} \frac{\mathrm{Im}[\langle \mathbf{k}\alpha'|\hat{v}_X|\mathbf{k}\alpha\rangle\langle\mathbf{k}\alpha|\hat{v}_Y|\mathbf{k}\alpha'\rangle]}{(E_{\mathbf{k}\alpha'} - E_{\mathbf{k}\alpha})^2}, \tag{36}$$

where $\hat{v}_{X/Y} = \partial\epsilon_\mathbf{k}/\partial k_{X/Y}$ are velocity operators along $\hat{X}/\hat{Y}$ directions and $|\mathbf{k}\alpha\rangle$ is the eigenvector of matrix $\epsilon_\mathbf{k}$ corresponding to the eigenenergy $E_{\mathbf{k}\alpha}$.

B. Magnetic phase diagrams

The mean-field saddle-point equations can be solved numerically with an ansatz magnetic order $\mathbf{Q} = (Q_X, Q_Y)$, and the saddle-point solution yields the mean-field ground-state energy $E_\mathbf{Q}$. The ground-state magnetic order should be obtained by finding $\mathbf{Q}$ that minimizes the mean-field energy $E_\mathbf{Q}$.

As suggested by the features of the RKKY interaction discussed in the last section, the s-p_X hybridization favors the order $\mathbf{Q} = (0, 0)$ or (π, π) and the Fermi surface nesting effect in p_X band favors the order $Q_X = \pi$. As a result, we consider only the paramagnetic, ferromagnetic [$\mathbf{Q} = (0, 0)$], AF [$\mathbf{Q} = (\pi, \pi)$], and CAF [$Q = (\pi, 0)$] orders in the slave-boson mean-field calculation. In Figs. 4(c) and 4(d) we plot $E_\mathbf{Q}$ versus $\mathbf{Q}$ for the parameters $(t_{sp}, t_s^Y, t_p^X, t_{sp}, \Delta_s) = (0.5, 0, 1, 0.5, 3)$ and $\phi = 0$, $\pi/2$, respectively. One can see that the relation between $E_\mathbf{Q}$ and $\mathbf{Q}$ in low-energy regions shown in Figs. 4(c) and 4(d) qualitatively agrees with the relation between the static magnetic susceptibility $\chi_\mathbf{Q}$ and $\mathbf{Q}$ in Figs. 4(a) and 4(b), and the ground-state magnetic orders obtained from both methods are the same. However, in the strong coupling t_{sp} regime, the magnetic orders from perturbation theory may not be justified since the perturbation theory is not valid in strong hybridization regime.

We plot the ground-state magnetic phase diagrams versus the coupling t_{sp} and phase ϕ in Fig. 6 with $(t_p^X, \Delta_s) = (1, 3)$. Note that the phase diagram from the present mean-field calculation is symmetric about $\phi = \pi$, so for convenience we plot only the phase diagrams in the region $0 < \phi < \pi$.

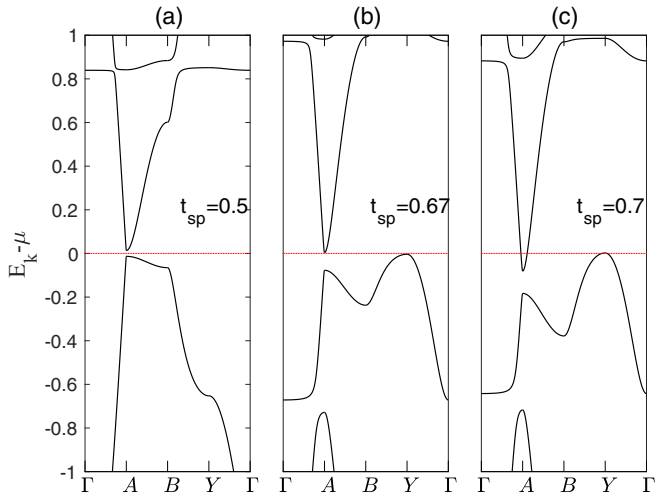

FIG. 7. The quasiparticle band obtained with slave-boson theory shows a transition from CAFKI phase to CAFKM phase at critical value $t_{sp}^c \simeq 0.67$ for $(t_s^Y, t_p^X, \Delta_s, \phi) = (0.1, 1, 3, 0.9\pi)$. The special k points are defined as $\Gamma = (0, 0)$, $A = (\pi/2, 0)$, $B = (\pi/2, \pi)$, $Y = (0, \pi)$.

Figure 6(a) shows the phase diagram with $t_s^Y = 0$, where the Hamiltonian can be transformed to the Kondo lattice Hamiltonian in weak hybridization regime as discussed previously. In weak hybridization regime $t_{sp} \lesssim 0.6$, the magnetic phase diagram qualitatively agrees with the perturbation result in Fig. 3. Namely, near $\phi = \pi/2$ the phase is AF Kondo insulator (AFKI), while near $\phi = 0$ and π the phase is CAF Kondo insulator (CAFKI). At large coupling regime, the slave-boson theory shows that for $\phi \approx \pi$, the phase evolves from CAFKI phase to the CAF Kondo metal (CAFKM) phase as t_{sp} increases (band structures are shown in Fig. 7), and then to ferromagnetic Kondo metal (FKM) phase. We note that the ferromagnetic order is not a ground-state order at half-filling in standard periodic Anderson model (with simple isotropic conduction band dispersion and k-independent hybridization) and may be ground state only away from half-filling in slave-boson mean-field calculation [63]. However, in the present CK model the emergence of ferromagnetism at half-filling is due to the anisotropic k-dependent hybridization function $V_{\mathbf{k}}$. In the region $\phi \approx 0$, the increase of t_{sp} does not affect the phase diagram much and the magnetic order is always CAF before magnetic moment decreases to zero. This asymmetry of the magnetic phase diagram about $\phi = \pi/2$ is in contrast to the symmetry of the magnetic phase diagram from RKKY interaction in the last section, where the second-order perturbation eliminates the p_X orbitals' degree of freedom. At very strong hybridization, the magnetic Kondo phases evolve into paramagnetic Kondo metal (PKM) phase, and further into paramagnetic Kondo insulator (PKI) phase, consistent with the Doniach diagram that the magnetic orders are fully suppressed in the strong coupling regime [61].

Figure 6(b) shows the magnetic phase diagram with $t_s^Y = 0.1$. The main difference in this case from that with $t_s^Y = 0$ [as shown in Fig. 6(a)] lies in weak hybridization t_{sp} regime. With $t_s^Y = 0.1$, the AF order disappears when $t_{sp} \lesssim 0.4$ but again appears at very weak t_{sp} and $\phi \approx \pi$. A comparison of magnetic orders with parameters $(t_p^X, t_{sp}, \Delta_s) = (1, 0.3, 3)$ for $t_s^Y = 0$ and ± 0.1 is shown in Fig. 3. One can see that only when $t_s^Y = 0$ the magnetic phase diagram from slave-boson mean-field theory agrees well with magnetic orders determined by RKKY interaction via perturbation in weak hybridization regime. In the strong hybridization regime, the effects of small t_s^Y on magnetism can be neglected compared to the large t_{sp}. Then, magnetic phase diagrams with $t_s^Y = 0.1$ and 0 are nearly the same.

The transition from PKM or topological PKI phase to trivial PKI phase, characterized by the gapless PKM line in [Figs. 6(a) and 6(b)], occurs when the renormalized s-orbital onsite energy increases so that $\beta_0 - \Delta_s$ satisfies $\beta_0 - \Delta_s > |z_+^2 t_s^Y + t_p^X|$. We note that the PKM has a vanishing indirect gap, but still has direct gap which is defined as the minimal energy difference of the upper and lower band states at fixed momentum (Fig. 7). However, as the energy minimum of the upper subbands equals to the energy maximum of the lower subbands, the Chern number of the PKM phase still denotes the topological invariant of the entire lower subbands.

For the paramagnetic Kondo phases obtained from slave-boson mean-field theory, the s-orbital onsite energy $-\Delta_s$ is renormalized from far below 0 to above 0 (the p_X orbital onsite energy is 0) and increases with the hybridization t_{sp} [see Fig. 8(a)], and similar results were also shown by Ref. [75]. In the weak bybridization limit, such property can be verified by the analytic solution provided in Refs. [65,76], where $\beta_0 - \Delta_s \propto e^2$ is given. In the strong t_{sp} regime, such property in our result can be understood in the following way. In the paramagnetic phase, the mean fields $z_- = 0$, $\beta = 0$, $p = 0$ and the number of order parameters can be reduced to two, i.e., z_+ and β_0, because e and p_0 can be viewed as functions of z_+ from Eqs. (26) and (30):

$$e = \frac{z_+}{\sqrt{2 - z_+^2}},$$
$$p_0 = \sqrt{1 - e^2}. \tag{37}$$

The Hamiltonian matrix can also be reduced to

$$\epsilon_k = \begin{pmatrix} z_+^2 \epsilon_{s\mathbf{k}} + \beta_0 & z_+ V_{\mathbf{k}} \\ z_+ V_{\mathbf{k}} & \epsilon_{p,\mathbf{k}} \end{pmatrix}. \tag{38}$$

From the formulas in Eq. (26) one can see that $e_i^2 + \sum_\mu \hat{p}_{i\mu}^\dagger \hat{p}_{i\mu} = e_i^2 + \sum_\sigma c_{i\sigma}^\dagger c_{i\sigma} = 1$ and the s-orbital occupation number equals to the pseudofermion occupation number since $d_i = 0$. As t_{sp} increases, the renormalized hybridization $z_+ t_{sp}$ and the holon number e^2 increases [see Fig. 8(a)], so the pseudofermion occupation number $\sum_\sigma c_{i\sigma}^\dagger c_{i\sigma}$ decreases. As a result, one can deduce β_0 should increase. Otherwise, if the renormalized onsite energy $\beta_0 - \Delta_s$ decreases or keeps unchanged, with the increase of $z_+ t_{sp}$, the pseudofermion occupation number $\sum_\sigma c_{i\sigma}^\dagger c_{i\sigma}$ in the fully filled lower band will increase towards $\frac{1}{2}$ for each spin component since the hybridization in the Hamiltonian matrix (38) is off-diagonal term and two eigenvectors of ϵ_k will approach $[1, 1]^T/\sqrt{2}$ and $[1, -1]^T/\sqrt{2}$ in the large t_{sp} limit.

The PKM to PKI transition that occurs at $\beta_0 - \Delta_s = 2(z_+^2 t_s^Y + t_p^X)$ can be identified by looking at special k points.

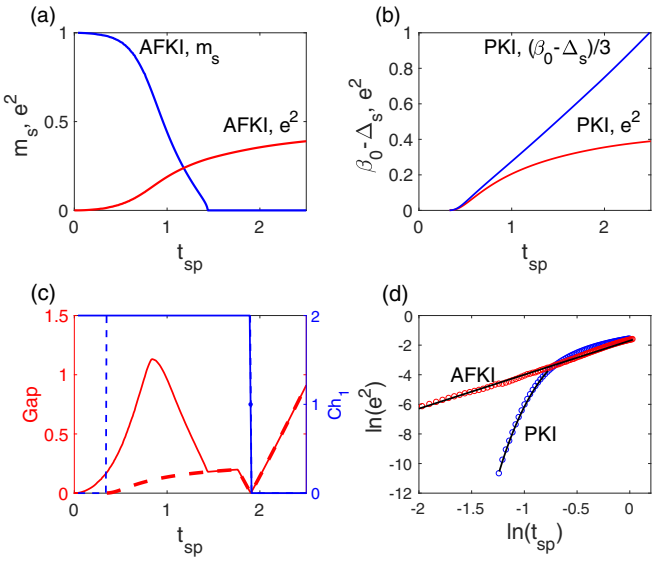

FIG. 8. Numerical results for the parameter condition $(t_s^Y, t_p^X, \Delta_s, \phi) = (0.1, 1, 3, 0.6\pi)$, computed with slave-boson theory. (a) The renormalized s-orbital onsite energy $\beta_0 - \Delta_s$ and holon number e^2 for PKI phase. (b) The staggered s-orbital magnetic moment m_s and holon number e^2 for the AFKI phase. (c) Quasiparticle gap and Chern number Ch_1 for the AFKI phase (solid lines) and PKI phase (dashed lines). The Chern number for both phases is different only in the weak t_{sp} regime. In the PKI phase, it shows $e^2 = 0$ when $\ln(t_{sp}) < -1.23$, and then both the quasiparticle gap and Ch_1 vanish. (d) The scaling $\ln(e^2)$ versus $\ln(t_{sp})$ for PKI/AFKI phase (circles) and their fitted curves (solid lines) in the weak t_{sp} regime. For the PKI phase, the fitted curve reads as $e^2 \propto t_{sp}^{-2} \exp(-1.078/t_{sp}^2)$ which ends for $\ln(t_{sp}) < -1.23$, while for the AFKI phase, the fitted line reads as $e^2 \propto t_{sp}^{2.29}$ which is nonzero for finite t_{sp}.

Near the transition point, the minimum energy of the upper paramagnetic band E^+ and maximum energy of the lower paramagnetic band E^- lie within high-symmetry k points $(\pi, 0)$ and $(0, \pi)$. For the k point $(\pi, 0)$, energies of upper and lower bands are

$$E^+(\pi, 0) = 2t_s^Y + \beta_0 - \Delta_s,$$
$$E^-(\pi, 0) = -2t_p^X. \tag{39}$$

For the k point $(\pi, 0)$, however, when $2(z_+^2 t_s^Y + t_p^X) < \beta_0 - \Delta_s$, the energies of upper and lower bands are

$$E^+(0, \pi) = -2t_s^Y + \beta_0 - \Delta_s,$$
$$E^-(0, \pi) = 2t_p^X, \tag{40}$$

while when $\beta_0 - \Delta_s < 2(z_+^2 t_s^Y + t_p^X)$, the energies of upper and lower bands are

$$E^+(0, \pi) = 2t_p^X,$$
$$E^-(0, \pi) = -2t_s^Y + \beta_0 - \Delta_s. \tag{41}$$

One can see from the above energies that when $t_s^Y = 0$, the paramagnetic phase will evolve from metal to insulator at the transition point, while when $t_s^Y > 0$, the paramagnetic phase is always insulator before and after the transition.

In the AFKI phase, the staggered magnetic moment m_s on s orbitals is plotted in Fig. 8(b). The m_s approaches local moment limit $m_s \to 1$ as $t_{sp} \to 0$, and decreases with the t_{sp} increasing until a continuous transition to the paramagnetic phase occurs. The magnetic moment m_p on p_X orbitals is always zero in the AFKI or CAFKI phase, for in our checkerboard superlattice each p_X orbital's four nearest s orbitals are in AF or CAF order. The effective Kondo interaction between s and p_X orbitals is spin-spin interaction, so particles on p_X orbitals experience frustrated effective magnetic field from s orbitals and thus have no magnetic moment.

C. QAH phase diagram

The QAH phase diagrams with $(t_p^X, \Delta_s) = (1, 3)$, $t_s^Y = 0$ and 0.1 are plotted in Figs. 6(a) and 6(b), respectively. With such parameters, in the single-particle regime without interaction, the QAH effect is trivial with $\mathrm{Ch}_1 = 0$ since $|\Delta_s| > 2|t_s^Y + t_p^X|$ [33]. However, in our CK model $U_s \to +\infty$ and with the slave-boson mean-field theory, the renormalization for s-orbital onsite energy which raises $-\Delta_s$ to $\beta_0 - \Delta_s$ may cause band crossing between s and p_X orbitals and thus possibly make the QAH phase nontrivial. In weak hybridization regime, as shown in Fig. 6, both AFKI and CAFKI phases are fully gapped and have quantized Chern number $\mathrm{Ch}_1 = 2$. When t_{sp} gradually increases, the CAFKI phase near $\phi = \pi$ evolves to gapless CAFKM phase and FKM phase with unquantized Chern number, while the CAFKI phase near $\phi = \pi$ and AFKI phase around $\phi = \pi/2$ are always gapped with $\mathrm{Ch}_1 = 2$. For the PKM or PKI phases in the large t_{sp} regime and on the left side of the PKM line, $|\beta_0 - \Delta_s| < 2|z_+^2 t_s^Y + t_p^X|$ is satisfied and total Chern number $\mathrm{Ch}_1 = 2$ with each spin component having Chern number 1. The PKM phase with $t_s^Y = 0$ is at the edge between gapless phase and gapped phase as discussed in the last subsection, for the maximum of the lower band equals to the minimum of the higher band, so the PKM phase has quantized Ch_1 although it is a metallic phase. On the right side of PKM line, the gap opens again with $|\beta_0 - \Delta_s| > 2|t_s^Y + t_p^X|$ and the QAH effect is trivial. The phases on the special line where $\phi = 0$ or π also have trivial band topology because the hybridization function $V_{\mathbf{k}}$ is real and the Berry curvature vanishes.

We now investigate the effects of magnetism on the QAH effect. The quasiparticle gap of the QAH phase opens due to the strongly renormalized s-p_X hybridization. In the Coleman slave-boson representation, the hybridization t_{sp} is renormalized in the form of et_{sp}, indicating that the nonzero effective hybridization is achieved with $e^2 > 0$ local moment for each s orbital. In the paramagnetic phase in KR slave-boson representation, e is just a monotonically increasing function of t_{sp}'s renormalization factor z_+ as shown by Eq. (30), so the above physical pictures also apply to the KR slave-boson representation. Figure 8(a) shows numerical results of the s-orbital holon number e^2 and renormalized onsite energy of the PKI phase with $(t_s^Y, t_p^X, \Delta_s, \phi) = (0.1, 1, 3, 0.6\pi)$. Below the critical hybridization $\ln(t_{sp}^c) \approx -1.23$, the holon number has a transition to $e^2 = 0$, representing the s and p_X orbitals are decoupled and gap closes [Fig. 8(c)], i.e., the CK transition described in the previous work [30]. The analytic result for paramagnetic slave-boson solutions for standard

periodic Anderson model [65,77] shows exponential relation $e^2 \propto J_K^{-1} \exp(1/J_K\rho)$ in the $t_{sp} \to 0$ limit, where the Kondo coupling satisfies $J_K \propto t_{sp}^2$ and a constant density of state for itinerant band has been assumed in their derivation. Although our CK model is anisotropic, the exponential relation $e^2 \propto J_K^{-1} \exp(1/J_K\rho)$ in the PKI phase can be fitted well when $t_{sp} > t_{sp}^c$ as shown in Fig. 8(d). The sudden decrease to zero of e in our numeric solution of the mean-field equations when $t_{sp} < t_{sp}^c$ may come from the inaccuracy of the numerical calculation, for e^2 decreases towards 0 so fast in the weak t_{sp} limit. However, since e^2 decreases so fast, we can still view the t_{sp}^c as a quasicritical point, and below this t_{sp}^c the renormalized hybridization can be regarded as 0 and the Ch_1 vanishes.

Compared to the PKI phase, in the magnetic Kondo phase the holon number e^2 does not decrease so fast and effective hybridization is enhanced in the weak hybridization limit. Among the magnetic Kondo phases, we found in our numerical results there is not much difference in the holon number e^2 between different types of magnetic orders. We plot holon number e^2 of the AFKI phase in Fig. 8(b) as an example, where e^2 is far more larger than that of the PKI phase in weak hybridization limit, implying the effective hybridization is enhanced compared to paramagnetic phase in such limit. Similar results were also shown by Refs. [62,63] for standard Anderson model. Another numerical study of standard one-dimensional periodic Anderson model with density-matrix renormalization group (DMRG) [65] found that the relation between e^2 and t_{sp} is power law $\ln e \propto \ln t_{sp}$ at weak t_{sp} with infinite large U_s in the Kondo regime, in contrast to the PKI phase obtained with slave-boson mean-field theory, where $e^2 \propto J_K^{-1} \exp(1/J_K\rho)$. It was also found that although the ground state has zero total spin, the antiferromagnetic correlation is strong. For the present CK model, we also plotted the fitted power-law relation $\ln e \propto \ln t_{sp}$ for the AFKI phase in Fig. 8(d), which qualitatively agrees with the DMRG result in Ref. [65]. As the magnetic Kondo phase is energetically more stable than the PKI phase in the weak hybridization regime, the CK transition in the PKI phase described in the previous work [30] will not occur in our CK model.

The present mean-field calculation also shows that different magnetic orders have different influences on QAH effect. The AF order always enhances the quasiparticle gap of the QAH phase compared to the paramagnetic phase, and we plot the comparison of gap between AFKI and PKI phase with $\phi = 0.6\pi$ in Fig. 8(c) as an example. In Fig. 8(c), similar to that shown in Refs. [63,64], the gap of the AFKI phase has a peak for $t_{sp} \approx 0.8$ that results from the increase of the self-consistent magnetic field β on s orbital (for detailed discussion, see Appendix). Note that other magnetic orders do not always enhance the gap. For CAF order, we obtain a CAFKI phase in the weak hybridization regime where the quasiparticle gap is enhanced, but as the hybridization increases, we obtain a CAFKI phase near $\phi \gtrsim 0$ and obtain a CAFKM phase near $\phi \approx \pi$ as shown from Fig. 6 with moderate t_{sp}. For the CAFKM phase, the quasiparticle is gapless and the Hall effect is not quantized any more. For ferromagnetic order, we always obtain a gapless FKM phase since the spin splitting is uniform in real space and thus the Hall effect is always not quantized.

D. Experimental measurement of the topology and strong correlation effects

The fully controllable cold atom experimental technologies including the Hall-effect measurement [78] and double-occupancy measurement [79,80] can enable us to identify the topology and influences of strong correlation on the CK phase. We now predict and discuss the observables including Hall conductance and double occupancy that can be affected by the topology and correlation effect, respectively. With the coexistence of magnetic order, these observables in the magnetic CK phase will be qualitatively different from those in the PKI phase.

The nontrivial band topology is determined by the existence of quasiparticle gap and band inversion. Having been discussed in the last subsection, the quasiparticle gap is affected by the existence of effective Kondo hybridization and the magnetic orders, while the band inversion is affected by the magnitude of the renormalized s-p_X onsite energy difference, which is controlled by the strength of t_{sp}. This leads to a rich QAH phase diagram. To identify the topological physics, one can either tune the magnitude of t_{sp} with phase ϕ fixed, or tune phase ϕ with the magnitude of t_{sp} fixed. In particular, one can tune the magnitude of t_{sp} with parameters $(t_s^Y, t_p^X, \Delta_s, \phi) = (0.1, 1, 3, 0.6\pi)$ being fixed. In the noninteracting regime, the s-orbital onsite energy lies far below the p_X orbital, and the phase is trivial irrespective of magnitude of t_{sp}. However, in the presence of strong repulsive interaction, the s-p_X onsite energy difference is strongly renormalized to a small quantity, with the effective hybridization being enhanced by the AF magnetic order in contrast to the paramagnetic phase, leading to the nontrivial QAH effect with $\mathrm{Ch}_1 = 2$ when t_{sp} is not too strong, as shown in Fig. 8(c). We note that for large enough t_{sp}, the onsite energy difference can be further renormalized, finally yielding a large magnitude again, and the phase can reenter the trivial regime, as shown in Figs. 8(b) and 8(c). Further, one can also tune ϕ from 0 to π and keep $(t_s^Y, t_p^X, t_{sp}, \Delta_s) = (0.1, 1, 0.77, 3)$ being fixed. In this case, the ground-state phases can be CAFKI, AFKI, CAFKI(M), or FKM phases with different ϕ (Figs. 6 and 9). Among these magnetic orders, the AF order always leads to an insulating phase with enhanced gap and QAH effect, the CAF

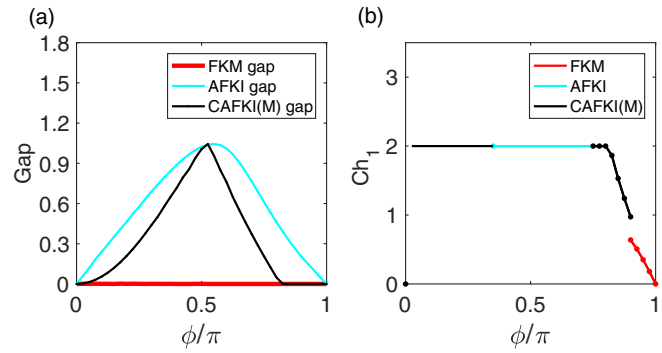

FIG. 9. Quasiparticle gaps, magnetic orders, and Chern number Ch_1 with $(t_s^Y, t_p^X, t_{sp}, \Delta_s) = (0.1, 1, 0.77, 3)$ obtained with slave-boson theory. (a) Quasiparticle gaps for three types of magnetic orders versus ϕ. (b) Ground-state magnetic order and first Chern number Ch_1 as a function of ϕ.

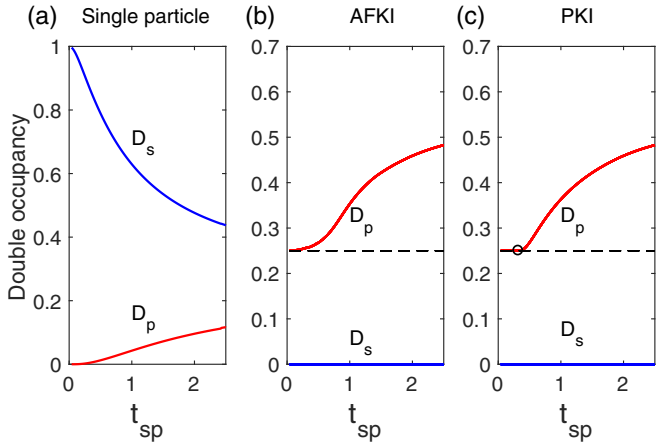

FIG. 10. Double-occupancy probability for s orbitals (D_s) and for p_X orbitals (D_p) with $(t_s^Y, t_p^X, \Delta_s, \phi) = (0.1, 1, 3, 0.6\pi)$. (a) Single-particle regime with $U_s = 0$. (b) AFKI phase in the regime with $U_s \to +\infty$. (c) PKI in the regime with $U_s \to +\infty$. The results in (b) and (c) are obtained with slave-boson theory. Note that D_p in (c) has a transition point labeled by a black circle. As seen in Fig. 8(a), when $t_{sp} \gtrapprox 1.45$, the AFKI magnetic moment vanishes and the system enters the PKI phase.

order may lead to insulating or metallic phase determined by t_{sp} and ϕ, while the ferromagnetic order always results in metallic phase without quantized Hall effect.

Concerning the strong correlation effects, we show the double occupancy D_p for p_X orbital and D_s for s orbital with $(t_s^Y, t_p^X, \Delta_s, \phi) = (0.1, 1, 3, 0.6\pi)$ in Fig. 10(b). We also calculated the double occupancy for the single-particle regime ($U_s = 0$) and PKI phase as a comparison in Figs. 10(a) and 10(c). Figure 10(a) differs from 10(b) and 10(c) for lack of correlation effect, while 10(b) differs from 10(c) without consideration of the magnetism. The D_p for noninteraction p_X orbital is calculated by Wick's theorem $D_p = n_{p\uparrow} n_{p\downarrow}$ for Figs. 10(a)–10(c). In the single-particle regime with $U_s = 0$ corresponding to Fig. 10(a), the onsite energy for s orbital lies below that of p_X orbital and thus the particle number and double occupancy on s orbitals are larger than that on p_X orbitals. Figures 10(b) and 10(c) correspond to the AFKI phase and PKI phase, respectively, in strong correlated regime with repulsive $U_s \to \infty$. Before the laser-assisted hybridization t_{sp} is induced, the s orbitals form a half-filled Mott insulator and the double occupancy D_s on s orbitals is suppressed to zero with the s-orbital onsite energy being renormalized to above p_X orbital due to strong U_s. Thus, in Figs. 10(b) and 10(c) D_p is greatly enhanced compared to that in the single-particle regime in Fig. 10(a). When hybridization t_{sp} is induced and effective hybridization exists, D_s keeps to be zero, while particles on s orbitals begin to pump into p_X orbitals, with the s-orbital onsite energy being further renormalized. The difference between Figs. 10(b) and 10(c) occurs in the weak hybridization t_{sp} limit. For the AFKI case with magnetic order, effective hybridization is enhanced and exists as long as $t_{sp} \neq 0$, while for the PKI phase the existence of effective hybridization needs the hybridization to exceed its quasicritical value t_{sp}^c, i.e., after the CK transition. Around the quasicritical t_{sp}^c, for the AFKI phase the D_p increases smoothly while for the PKI phase the D_p starts to increase abruptly at $t_{sp} \gtrsim t_{sp}^c$, showing the difference between emergence of the magnetic and paramagnetic CK phases.

V. CONCLUSIONS

In this work, we have examined the Chern Kondo insulator by revisiting its realization and studied the magnetic effects on the Chern Kondo phases. An improved scheme for the realization of Chern Kondo insulator is proposed, solving the challenges in the previous realization. The Ruderman-Kittel-Kasuya-Yoshida magnetic interaction is analyzed at weak hybridization limit, with the anisotropic magnetic effects being discussed. We further systematically studied the paramagnetic and magnetic phases coexisting with Kondo hybridization based on slave-boson theory and mapped out the full magnetic and correlated QAH phase diagrams. The rich phases, including the paramagnetic/magnetic Kondo insulating phases and magnetic Kondo metallic phases, have been obtained and investigated in detail. Interestingly, the effective Kondo hybridization can be typically strengthened by taking into account magnetic effects. In particular, we showed that the existence of antiferromagnetic order enhances the Kondo phase, with the topological bulk gap being increased compared with that in the paramagnetic regime. On the other hand, the Kondo phases coexisting with collinear antiferromagnetic order have metal-insulator transition determined by the strength and phase of hybridization, which is absent in the paramagnetic Kondo phase. Moreover, in the large hybridization regime, the bulk phase may eventually enter the paramagnetic Kondo insulating states, which manifests that the magnetic orders are fully suppressed in the strongly Kondo regime. The Chern Kondo phases can be detected by measuring the Chern number of bulk topology and the double occupancy, which are achievable in cold atom experiments. The rich strongly correlated and topological physics may motivate further studies of the Chern Kondo phases in theory and experiment.

ACKNOWLEDGMENT

We appreciate the discussion with H. Chen. This work was supported by the National Key R&D Program of China (Grant No. 2016YFA0301604), National Nature Science Foundation of China (under Grants No. 11574008 and No. 11761161003), and the Thousand-Young-Talent Program of China.

APPENDIX

1. The s-p_X hopping integrals from laser-assisted tunneling in the previous realization

In this section we will evaluate the hopping integrals for original laser-assisted tunneling in Fig. 1(a):

$$J_1 = \int d^2r\, \psi^p_{n,m}(x,y)\psi^s_{n+1,m}(x,y)e^{ik_R(y-m)}e^{ik_R m},$$

$$J_2 = \int d^2r\, \psi^p_{n+1,m+1}(x,y)\psi^s_{n+1,m}(x,y)e^{-ik_R[y-(m+\frac{1}{2})]} \times e^{-ik_R(m+\frac{1}{2})},$$

$$J_3 = \int d^2r\, \psi^p_{n+1,m+1}(x,y)\psi^s_{n,m+1}(x,y)e^{ik_R[y-(m+1)]}e^{ik_R(m+1)},$$
$$J_4 = \int d^2r\, \psi^p_{n,m}(x,y)\psi^s_{n,m+1}(x,y)e^{-ik_R[y-(m+\frac{1}{2})]}e^{-ik_R(m+\frac{1}{2})}. \tag{A1}$$

Here, $\psi^p_{n,m}(x,y)$ and $\psi^s_{n,m}(x,y)$ are real maximally localized Wannier functions for p_X (s) orbitals, (n,m) is the coordinate of lattice site, and $\psi^p_{0,0}(x,y)/\psi^s_{0,0}(x,y)$ are odd/even functions, respectively. We also have $\psi_{n,m}(x,y) = \psi_{0,0}(x-n, y-m)$, then the integrals can be simplified:

$$\begin{aligned} I_1 &= \int d^2r\, \psi^p_{n,m}(x,y)\psi^s_{n+1,m}(x,y)e^{ik_R(y-m)} \\ &= \int d^2r\, \psi^p_{0,0}(x,y)\psi^s_{1,0}(x,y)e^{ik_Ry}, \\ I_3 &= \int d^2r\, \psi^p_{n+1,m+1}(x,y)\psi^s_{n,m+1}(x,y)e^{ik_R(y-(m+1))} \\ &= -\int d^2r\, \psi^p_{0,0}(x,y)\psi^s_{1,0}(x,y)e^{-ik_Ry}. \end{aligned} \tag{A2}$$

In the above formulas, we have used the property of integral:

$$\begin{aligned} \int dr^2 f(x,y) &= \int_{-\infty}^{+\infty} dx \int_{-\infty}^{+\infty} dy\, f(x,y) \\ &= \int_{-\infty}^{+\infty} dx \int_{-\infty}^{+\infty} dy\, f(-x,-y) \\ &= \int dr^2 f(-x,-y). \end{aligned} \tag{A3}$$

Decomposing the complex integral into real and imaginary parts, we can obtain the relation between I_1 and I_3:

$$\begin{aligned} I_1 &= +\int d^2r\, \psi^p_{0,0}(x,y)\psi^s_{1,0}(x,y)\cos(k_Ry) \\ &\quad + i\int d^2r\, \psi^p_{0,0}(x,y)\psi^s_{1,0}(x,y)\sin(k_Ry) = I_a, \\ I_3 &= -\int d^2r\, \psi^p_{0,0}(x,y)\psi^s_{1,0}(x,y)\cos(k_Ry) \\ &\quad + i\int d^2r\, \psi^p_{0,0}(x,y)\psi^s_{1,0}(x,y)\sin(k_Ry) = -I^*_a. \end{aligned} \tag{A4}$$

Similarly,

$$\begin{aligned} I_2 &= \int d^2r\, \psi^p_{n+1,m+1}(x,y)\psi^s_{n+1,m}(x,y)e^{-ik_R[y-(m+\frac{1}{2})]} \\ &= -\int d^2r\, \psi^p_{0,0}\left(x, y+\frac{1}{2}\right)\psi^s_{0,0}\left(x, y-\frac{1}{2}\right)e^{ik_Ry}, \\ I_4 &= \int d^2r\, \psi^p_{n,m}(x,y)\psi^s_{n,m+1}(x,y)e^{-ik_R[y-(m+\frac{1}{2})]} \\ &= \int d^2r\, \psi^p_{0,0}\left(x, y+\frac{1}{2}\right)\psi^s_{0,0}\left(x, y-\frac{1}{2}\right)e^{-ik_Ry}. \end{aligned} \tag{A5}$$

Decomposing these two numbers into real and imaginary parts, we can obtain the relation between I_2 and I_4:

$$\begin{aligned} I_2 &= -\int d^2r\, \psi^p_{0,0}\left(x, y+\frac{1}{2}\right)\psi^s_{0,0}\left(x, y-\frac{1}{2}\right)\cos(k_Ry) \\ &\quad - i\int d^2r\, \psi^p_{0,0}\left(x, y+\frac{1}{2}\right)\psi^s_{0,0}\left(x, y-\frac{1}{2}\right)\sin(k_Ry) \\ &= -I^*_b, \\ I_4 &= +\int d^2r\, \psi^p_{0,0}\left(x, y+\frac{1}{2}\right)\psi^s_{0,0}\left(x, y-\frac{1}{2}\right)\cos(k_Ry) \\ &\quad - i\int d^2r\, \psi^p_{0,0}\left(x, y+\frac{1}{2}\right)\psi^s_{0,0}\left(x, y-\frac{1}{2}\right)\sin(k_Ry) \\ &= I_b. \end{aligned} \tag{A6}$$

2. Effective Kondo lattice Hamiltonian

The effective Kondo lattice Hamiltonian is derived through perturbation theory when s-p_X hybridization is weak and the s-orbital onsite energy lies far below the p_X orbital. Here, we provide detailed derivation of the Kondo lattice Hamiltonian

$$H_{\mathrm{KL}} = \sum_{\mathbf{k}\sigma} \epsilon_{p\mathbf{k}} p^\dagger_{X\mathbf{k}\sigma} p_{X\mathbf{k}\sigma} + \sum_{i,\mathbf{k},\mathbf{k}'} J_{\mathbf{k},\mathbf{k}',i}\mathbf{S}_i \cdot \mathbf{s}_{\mathbf{k}\mathbf{k}'} \tag{A7}$$

from the original Hamiltonian

$$\begin{aligned} H &= H_1 + H', \\ H_1 &= \sum_{i\sigma}\left[-\Delta_s s^\dagger_{i\sigma}s_{i\sigma} + t^X_p p^\dagger_{Xi\sigma}p_{Xi\pm\hat{X}\sigma}\right] + \sum_i U_s \hat{n}_{si\uparrow}\hat{n}_{si\downarrow}, \\ H' &= \sum_{\mathbf{k},i} \frac{V_{\mathbf{k}}e^{-i\mathbf{k}\cdot\mathbf{R}_i}}{\sqrt{N}} s^\dagger_{i\sigma}p_{Xk\sigma} + \mathrm{H.c.}, \end{aligned} \tag{A8}$$

and the definition of the effective Hamiltonian

$$H_p(E) = PHP - PHQ\frac{1}{QHQ-E}QHP, \tag{A9}$$

where the projection operator P project states onto subspace with each s orbital singly occupied and $Q = 1 - P$.

We separate H' into $H' = H_+ + H_-$, where $H_+ = \sum_{\mathbf{k},i} N^{-1/2}V_{\mathbf{k}}e^{-i\mathbf{k}\cdot\mathbf{R}_i}s^\dagger_{i\sigma}p_{Xk\sigma}$ and $H_- = \sum_{\mathbf{k},i} N^{-1/2}V_{\mathbf{k}}e^{i\mathbf{k}\cdot\mathbf{R}_i}p^\dagger_{Xk\sigma}s_{i\sigma}$. The operator H_+ increases one particle on s orbitals and H_- decreases one particle on s orbitals. Consider the approximation that replaces the unknown E with the unperturbed energy E_0. The formulas become

$$\begin{aligned} PH_1Q &= 0, \\ PH'P &= 0, \\ QH'Q &= 0, \end{aligned} \tag{A10}$$

and the effective Hamiltonian can be simplified to the form

$$H_p(E) \approx P(H_1 + H_+ + H_-)P - P(H_1 + H_+ + H_-)Q\frac{1}{QHQ - E_0}Q(H_1 + H_+ + H_-)P$$
$$= PH_1P - PH_+Q\frac{1}{QH_1Q - E_0}QH_-P - PH_-Q\frac{1}{QH_1Q - E_0}QH_+P. \tag{A11}$$

Substituting H_1, H_+, and H_- into above formula yields the form

$$H_p(E) = \sum_{\mathbf{k}\sigma}\epsilon_{p\mathbf{k}}p^\dagger_{X\mathbf{k}\sigma}p_{X\mathbf{k}\sigma} - \sum_{\substack{\mathbf{k},\mathbf{k}'\\ i,\sigma,\sigma'}}\frac{V^*_{\mathbf{k}}V_{\mathbf{k}'}e^{i(\mathbf{k}-\mathbf{k}')\cdot\mathbf{R}_i}}{N}\frac{s^\dagger_{i\sigma'}p_{X\mathbf{k}'\sigma'}p^\dagger_{X\mathbf{k}\sigma}s_{i\sigma}}{\epsilon_{p\mathbf{k}} + \Delta_s} - \sum_{\substack{\mathbf{k},\mathbf{k}'\\ i,\sigma,\sigma'}}\frac{V^*_{\mathbf{k}}V_{\mathbf{k}'}e^{i(\mathbf{k}'-\mathbf{k})\cdot\mathbf{R}_i}}{N}\frac{p^\dagger_{X\mathbf{k}'\sigma'}s_{i\sigma'}s^\dagger_{i\sigma}p_{X\mathbf{k}\sigma}}{U_s - \epsilon_{p\mathbf{k}} - \Delta_s}. \tag{A12}$$

Here, we have discarded the onsite energy $-N\Delta_s$ for s orbitals, for it is a constant in the subspace P. The third term in the above formula can be omitted since we only consider the infinitely large U_s limit. Using the identity $s^\dagger_{i\sigma'}p_{Xk\sigma'}p^\dagger_{Xk\sigma}s_{i\sigma} = s^\dagger_{i\sigma'}s_{i\sigma}(\delta_{\sigma\sigma'}\delta_{kk'} - p^\dagger_{Xk\sigma}p_{Xk'\sigma'})$, the effective Hamiltonian reads as

$$H_p(E) = \sum_{\mathbf{k}\sigma}\epsilon_{p\mathbf{k}}p^\dagger_{X\mathbf{k}\sigma}p_{X\mathbf{k}\sigma} + \sum_{\substack{\mathbf{k},\mathbf{k}'\\ i,\sigma,\sigma'}}\frac{V^*_{\mathbf{k}}V_{\mathbf{k}'}e^{i(\mathbf{k}-\mathbf{k}')\cdot\mathbf{R}_i}}{N}\frac{s^\dagger_{i\sigma'}s_{i\sigma}p^\dagger_{X\mathbf{k}\sigma}p_{X\mathbf{k}'\sigma'}}{\epsilon_{p\mathbf{k}} + \Delta_s} - \sum_{\mathbf{k},i,\sigma}V^*_{\mathbf{k}}V_{\mathbf{k}}\frac{s^\dagger_{i\sigma}s_{i\sigma}}{\epsilon_{p\mathbf{k}} + \Delta_s}. \tag{A13}$$

The third term in the above formula is also a constant in the subspace P. Defining the spin density operators $\mathbf{S}_i = s^\dagger_{i\sigma'}\boldsymbol{\tau}_{\sigma'\sigma}s_{i\sigma}/2$, $\mathbf{s}_{\mathbf{k},\mathbf{k}'} = p^\dagger_{X\mathbf{k}\sigma'}\boldsymbol{\tau}_{\sigma'\sigma}p_{X\mathbf{k}'\sigma}/2$ where $\boldsymbol{\tau}$ is the vector formed by three Pauli matrices, we obtain the identities

$$\begin{aligned}
&s^\dagger_{i\uparrow}s_{i\downarrow}p^\dagger_{Xk\downarrow}p_{Xk'\uparrow} = S^+_i s^-_{kk'},\\
&s^\dagger_{i\downarrow}s_{i\uparrow}p^\dagger_{Xk\uparrow}p_{Xk'\downarrow} = S^-_i s^+_{kk'},\\
&s^\dagger_{i\uparrow}s_{i\uparrow}p^\dagger_{Xk\uparrow}p_{Xk'\uparrow} + s^\dagger_{i\downarrow}s_{i\downarrow}p^\dagger_{Xk\downarrow}p_{k'\downarrow} = \tfrac{1}{2}(p^\dagger_{Xk\uparrow}p_{Xk'\uparrow} + p^\dagger_{Xk\downarrow}p_{Xk'\downarrow}) + 2S^z_i s^z_{kk'}.
\end{aligned} \tag{A14}$$

The potential scattering term $p^\dagger_{Xk\uparrow}p_{Xk'\uparrow} + p^\dagger_{Xk\downarrow}p_{Xk'\downarrow}$ in the third line can be omitted if we only care about the phenomena about magnetism. Finally, we obtain the effective Kondo lattice Hamiltonian:

$$H_{\mathrm{KL}} = \sum_{\mathbf{k}\sigma}\epsilon_{p\mathbf{k}}p^\dagger_{X\mathbf{k}\sigma}p_{X\mathbf{k}\sigma} + \sum_{i,\mathbf{k},\mathbf{k}'}2J_{\mathbf{k},\mathbf{k}',i}\mathbf{S}_i\cdot\mathbf{s}_{\mathbf{k}\mathbf{k}'}. \tag{A15}$$

Here, the anisotropic k-dependent Kondo coupling $J_{\mathbf{k},\mathbf{k}',i} = \frac{1}{N}\frac{V^*_{\mathbf{k}}V_{\mathbf{k}'}e^{i(\mathbf{k}-\mathbf{k}')\cdot\mathbf{R}_i}}{\epsilon_{p\mathbf{k}}+\Delta_s}$ contains the information of the hybridization between s and p_X orbitals.

3. RKKY interaction

To derive the RKKY interaction, we take the p_X orbital hopping terms as unperturbed Hamiltonian and take the Kondo interaction as the perturbation. We separate the Kondo interaction into three terms, and the Kondo lattice Hamiltonian reads as

$$H_{\mathrm{KL}} = \sum_{k}\epsilon_{pk}p^\dagger_{Xk\sigma}p_{Xk\sigma} + \sum_{k,k',i}J_{k,k',i}\left(S^-_i p^\dagger_{Xk\uparrow}p_{Xk'\downarrow} + S^+_i p^\dagger_{Xk\downarrow}p_{Xk'\uparrow} + S^z_i\sum_\sigma\sigma p^\dagger_{Xk\sigma}p_{Xk'\sigma}\right). \tag{A16}$$

Now, we define three components of the Kondo interaction $H_- = \sum_{k,k',i}J_{k,k',i}S^-_i p^\dagger_{Xk\uparrow}p_{Xk'\downarrow}$, $H_+ = \sum_{k,k',i}J_{k,k',i}S^+_i p^\dagger_{Xk\downarrow}p_{Xk'\uparrow}$, and $H_z = \sum_{k,k',i}J_{k,k',i}S^z_i\sum_\sigma\sigma p^\dagger_{Xk\sigma}p_{Xk'\sigma}$. We also define the projection operator P_0 that projects the original Hilbert space of Kondo lattice onto the subspace with a ground-state Fermi sea formed by p_X orbital degree of freedom, i.e., $\hat{n}_{pk\sigma} = 1$ when $\epsilon_{p,k} < \epsilon_{p,k_F}$, and $\hat{n}_{pk\sigma} = 0$ when $\epsilon_{p,k} > \epsilon_{p,k_F}$. The states in subspace $Q_0 = 1 - P_0$ have particle-type or hole-type excitations in p_X orbital degree of freedom.

Following the steps in the derivation of the Kondo lattice Hamiltonian, the effective Hamiltonian H_{p_0} reads as

$$H_{p_0} = P_0H_{\mathrm{KL}}P_0 + P_0H_zQ_0\frac{1}{Q_0H_{\mathrm{KL}}Q_0 - E_0}Q_0H_zP_0 + P_0H_+Q_0\frac{1}{Q_0H_{\mathrm{KL}}Q_0 - E_0}Q_0H_-P_0 + P_0H_-Q_0\frac{1}{Q_0H_{\mathrm{KL}}Q_0 - E_0}Q_0H_+P_0. \tag{A17}$$

The first term, $P_0 H_{\rm KL} P_0 = \sum_{\epsilon_{pk}<\epsilon_{pk_F}} 2\epsilon_{pk}$, is a constant term and does not affect the magnetism. The second term takes the form

$$\begin{aligned} P_0 H_z Q_0 \frac{1}{Q_0 H_{\rm KL} Q - E_0} Q_0 H_z P_0 &= \sum_{kk'ij} J_{kk'i} J_{k'kj} S_i^z S_j^z (p_{k\uparrow}^\dagger p_{k'\uparrow} p_{k'\uparrow}^\dagger p_{k\uparrow} + p_{k\downarrow}^\dagger p_{k'\downarrow} p_{k'\downarrow}^\dagger p_{k\downarrow})/(\epsilon_{p,k'} - \epsilon_{p,k}) \\ &= \sum_{kk'ij} 2 J_{kk'i} J_{k'kj} S_i^z S_j^z [n_{p,k}(1 - n_{p,k'})]/(\epsilon_{p,k'} - \epsilon_{p,k}) \\ &= \sum_{ijkk'} 2 J_{kk'i} J_{k'kj} S_i^z S_j^z [n_{p,k} - n_{p,k'}]/(\epsilon_{p,k'} - \epsilon_{p,k}). \end{aligned} \tag{A18}$$

Similarly, the third term reads as

$$P_0 H_+ Q_0 \frac{1}{Q_0 H_{\rm KL} Q - E_0} Q_0 H_- P_0 = \sum_{ijkk'} 2 J_{kk'i} J_{k'kj} S_i^+ S_j^- [n_{p,k} - n_{p,k'}]/(\epsilon_{p,k'} - \epsilon_{p,k}), \tag{A19}$$

and the fourth term reads as

$$P_0 H_- Q_0 \frac{1}{Q_0 H_{\rm KL} Q - E_0} Q_0 H_+ P_0 = \sum_{ijkk'} 2 J_{kk'i} J_{k'kj} S_i^- S_j^+ [n_{p,k} - n_{p,k'}]/(\epsilon_{p,k'} - \epsilon_{p,k}). \tag{A20}$$

Finally, we obtain the RKKY interaction

$$H_{\rm RKKY} = \sum_{i,j} 2J(X_i - X_j, Y_i - Y_j) \mathbf{S}_i \cdot \mathbf{S}_j, \tag{A21}$$

where coupling coefficient takes the form

$$J(X_i - X_j, Y_i - Y_j) = \sum_{k,k'} J_{k,k',j} J_{k',k,j} = \sum_{\mathbf{k},\mathbf{k}'} \frac{4\cos[(\mathbf{k} - \mathbf{k}') \cdot (\mathbf{R}_i - \mathbf{R}_j)]}{N^2} |V_{\mathbf{k}}|^2 |V_{\mathbf{k}'}|^2 \frac{1}{\epsilon_{p\mathbf{k}} + \Delta_s} \frac{1}{\epsilon_{p\mathbf{k}'} + \Delta_s} \frac{n_{p,\mathbf{k}} - n_{p,\mathbf{k}'}}{\epsilon_{p,\mathbf{k}} - \epsilon_{p,\mathbf{k}'}}. \tag{A22}$$

4. Slave-boson mean-field Hamiltonian

In this section, we first review the spin-rotation invariant slave-boson formulas introduced in Ref. [73] and then provide the derivation of mean-field Hamiltonian of the CK model following [62,74]. The spin-rotation invariant type slave-boson theory [73] is convenient to describe various magnetic orders. Furthermore, it will give better results when considering fluctuations around mean-field solutions [73], although our treatment is only restricted to mean-field level.

The purpose of the slave-boson mean-field theory is to construct composite particle states and Hamiltonian operator that are equivalent to the original states and Hamiltonian, and then take the boson fields to be mean fields as an approximation. In the spin-rotation invariant slave-boson theory [73], auxiliary bosonic and fermionic operators are introduced. On the one hand, the slave-boson operators $\hat{e}$, $\hat{d}$, $\hat{p}_0$, $\hat{\mathbf{p}} = (\hat{p}_1, \hat{p}_2, \hat{p}_3)$ that obey bosonic commutation relation are introduced. Here, $\hat{e}$, $\hat{d}$ correspond to hole and doubly occupied states; scalar ($S = 0$) field $\hat{p}_0$ and vector ($S = 1$) field $\hat{\mathbf{p}} = (\hat{p}_1, \hat{p}_2, \hat{p}_3)$ correspond to the singly occupied state. $\hat{e}$, $\hat{d}$, $\hat{p}_0$ transform as a scalar under spin rotation and $\hat{\mathbf{p}}$ transforms as a vector. On the other hand, the $S = \frac{1}{2}$ pseudofermion operators $c_{i\sigma}$ obey the fermionic commutation relation.

The holon and doublon states can be constructed directly:

$$|0\rangle = \hat{e}^\dagger |{\rm vac}\rangle, \quad |\uparrow\downarrow\rangle = \hat{d}^\dagger c_\uparrow^\dagger c_\downarrow^\dagger |{\rm vac}\rangle, \tag{A23}$$

where $|{\rm vac}\rangle$ is the vacuum for both boson and fermion states. Concerning the singly occupied states, there are two ways to construct a composite $S = \frac{1}{2}$ state via combining the slave-boson operators $\hat{p}_0$, $\hat{p}_1$, $\hat{p}_2$, $\hat{p}_3$ with pseudofermion operator $c_{i\sigma}$. The first type composite $S = \frac{1}{2}$ states are

$$\left|\tfrac{1}{2}, \sigma\right\rangle = \hat{p}_0^\dagger c_\sigma^\dagger |{\rm vac}\rangle. \tag{A24}$$

Alternatively, we can define $S = 1$ eigenstates of vector $\hat{p}$ bosons:

$$\begin{aligned} &\hat{p}_{1,1}^\dagger = \frac{1}{\sqrt{2}}(\hat{p}_1^\dagger - i\hat{p}_2^\dagger), \quad \hat{p}_{1,-1}^\dagger = -\frac{1}{\sqrt{2}}(\hat{p}_1^\dagger + i\hat{p}_2^\dagger), \\ &\hat{p}_{1,0}^\dagger = -\hat{p}_3^\dagger, \end{aligned} \tag{A25}$$

and with the Clebsch-Gordan coefficients, we obtain the second-type composite $S = \frac{1}{2}$ states

$$\begin{aligned} \left|\frac{1}{2}, \frac{1}{2}\right\rangle &= -\frac{1}{\sqrt{3}} \hat{p}_{1,0}^\dagger c_\uparrow^\dagger |{\rm vac}\rangle + \frac{\sqrt{2}}{\sqrt{3}} \hat{p}_{1,1}^\dagger c_\downarrow^\dagger |{\rm vac}\rangle, \\ \left|\frac{1}{2}, -\frac{1}{2}\right\rangle &= \frac{1}{\sqrt{3}} \hat{p}_{1,0}^\dagger c_\downarrow^\dagger |{\rm vac}\rangle - \frac{\sqrt{2}}{\sqrt{3}} \hat{p}_{1,-1}^\dagger c_\uparrow^\dagger |{\rm vac}\rangle. \end{aligned} \tag{A26}$$

Moreover, the combination of the above two types also results in a spin-$\frac{1}{2}$ particle via defining

$$|\sigma\rangle = \sum_{\sigma'} \hat{p}_{\sigma\sigma'}^\dagger c_{\sigma'}^\dagger |{\rm vac}\rangle, \tag{A27}$$

where $\hat{p}_{\sigma\sigma'}^\dagger$ is the matrix elements of

$$\underline{\hat{p}}^\dagger = \begin{bmatrix} a\hat{p}_0^\dagger + b\hat{p}_3^\dagger & b(\hat{p}_1^\dagger - i\hat{p}_2^\dagger) \\ b(\hat{p}_1^\dagger + i\hat{p}_2^\dagger) & a\hat{p}_0^\dagger - b\hat{p}_3^\dagger \end{bmatrix}. \tag{A28}$$

From normalization condition, we obtain $a^2 + 3b^2 = 1$ and we take $a = b = \frac{1}{2}$, then

$$\hat{p}^\dagger_{\sigma\sigma'} = \frac{1}{2}\sum_{\mu=0}^{3}\hat{p}^\dagger_\mu \tau_{\mu,\sigma\sigma'}, \quad \hat{p}_{\sigma\sigma'} = \frac{1}{2}\sum_{\mu=0}^{3}\hat{p}_\mu \tau_{\mu,\sigma\sigma'}. \tag{A29}$$

To project out the unphysical states in the extended Hilbert space, the following constraints are necessary:

$$\begin{aligned} &\hat{e}^\dagger_i\hat{e}_i + \hat{d}^\dagger_i\hat{d}_i + \sum_\mu \hat{p}^\dagger_{i\mu}\hat{p}_{i\mu} - 1 = 0, \\ &\sum_\sigma c^\dagger_{i\sigma}c_{i\sigma} - \sum_\mu \hat{p}^\dagger_{i\mu}\hat{p}_{i\mu} - 2\hat{d}^\dagger_i\hat{d}_i = 0, \\ &\sum_{\sigma\sigma'} \boldsymbol{\tau}_{\sigma\sigma'}c^\dagger_{i\sigma'}c_{i\sigma} - \hat{p}_{i0}\hat{\mathbf{p}}^\dagger_i - \hat{\mathbf{p}}^\dagger_i\hat{p}_{i0} + i(\hat{\mathbf{p}}^\dagger_i \times \hat{\mathbf{p}}_i) = 0. \end{aligned} \tag{A30}$$

Alternatively, they can be written as

$$\begin{aligned} &\hat{e}^\dagger_i\hat{e}_i + \hat{d}^\dagger_i\hat{d}_i + \sum_\mu \hat{p}^\dagger_{i\mu}\hat{p}_{i\mu} = 1, \\ &c^\dagger_{i\sigma'}c_{i\sigma} = 2\sum_{\sigma_1}\hat{p}^\dagger_{i\sigma_1\sigma}\hat{p}_{i\sigma'\sigma_1} + \delta_{\sigma\sigma'}\hat{d}^\dagger_i\hat{d}_i, \end{aligned} \tag{A31}$$

where the first constraint means that each physical state has one boson, and the second constraint guarantees that correct boson states are attached to the corresponding fermion states. One can easily check that with the above constraints and the formulas $[p_{\sigma\sigma'}, p^\dagger_{\sigma'\sigma}] = \frac{1}{2}$ and $p_{\sigma\bar{\sigma}}p^\dagger_{\sigma\bar{\sigma}}|\text{vac}\rangle = 0$, only the following four physical states are left:

$$\begin{aligned} |\uparrow\rangle &= \hat{p}^\dagger_{\uparrow\uparrow}c^\dagger_\uparrow|\text{vac}\rangle + \hat{p}^\dagger_{\uparrow\downarrow}c^\dagger_\downarrow|\text{vac}\rangle, \\ |\downarrow\rangle &= \hat{p}^\dagger_{\downarrow\uparrow}c^\dagger_\uparrow|\text{vac}\rangle + \hat{p}^\dagger_{\downarrow\downarrow}c^\dagger_\downarrow|\text{vac}\rangle, \\ |0\rangle &= \hat{e}^\dagger|\text{vac}\rangle, \\ |\uparrow\downarrow\rangle &= \hat{d}^\dagger c^\dagger_\uparrow c^\dagger_\downarrow|\text{vac}\rangle, \end{aligned} \tag{A32}$$

where the former two states are singly occupied states, the third is holon, and the last is doublon. The local s-orbital operators s_σ in our CK model are represented by $s_\sigma = \sum_{\sigma'}\hat{z}_{\sigma\sigma'}c_{\sigma'}$, with the matrix $\underline{z}$ defined as

$$\hat{\underline{z}} = \hat{e}^\dagger \underline{L}\underline{R}\hat{\underline{p}} + \hat{\underline{p}}^\dagger \underline{L}\underline{R}\hat{d}, \tag{A33}$$

where

$$\underline{L} = [(1 - \hat{d}^\dagger\hat{d})\underline{1} - 2\underline{\hat{p}}^\dagger\underline{\hat{p}}]^{-\frac{1}{2}}, \quad \underline{R} = [(1 - \hat{e}^\dagger\hat{e})\underline{1} - 2\underline{\hat{p}}^\dagger\underline{\hat{p}}]^{-\frac{1}{2}}. \tag{A34}$$

Here, $\underline{1}$ is a 2×2 identity matrix, and $\underline{\hat{p}}_{\sigma\sigma'} = (\hat{T}\underline{\hat{p}}\hat{T}^{-1})_{\sigma\sigma'} = \sigma\sigma'\hat{p}_{\bar{\sigma}'\bar{\sigma}}$ is time reversal of $\hat{p}_{\sigma\sigma'}$. The operator $\underline{L}\underline{R}$ in Eq. (A33) equals to identity matrix and acts as a renormalization factor in the mean-field approximation. For each s orbital at site $\mathbf{R}_i$, a set of above auxiliary operators are induced with index i labeling their sites. In terms of the auxiliary operators and writing the constraints in the form of Lagrange multiplier fields, the CK Hamiltonian reads as

$$\begin{aligned} H = \sum_{i\sigma}\Bigg[&\sum_{\sigma'\sigma''} t^Y_s \hat{z}^\dagger_{i\sigma\sigma'}\hat{z}_{i\pm\hat{Y}\sigma''\sigma}c^\dagger_{i\sigma'}c_{i\pm\hat{Y}\sigma''} - \Delta_s c^\dagger_{i\sigma}c_{i\sigma} + t^X_p p^\dagger_{Xi\sigma}p_{Xi\pm\hat{X}\sigma}\Bigg] + \Bigg[\sum_{\langle ij\rangle\sigma} F(\mathbf{r})\hat{z}^\dagger_{i\sigma\sigma'}c^\dagger_{i\sigma'}p_{Xj\sigma}\delta_{j,i+\mathbf{r}} + \text{H.c.}\Bigg] \\ &+ \sum_i\Bigg[U_s\hat{d}^\dagger_i\hat{d}_i + \alpha_i\left(\hat{e}^\dagger_i\hat{e}_i + \hat{d}^\dagger_i\hat{d}_i + \sum_\mu \hat{p}^\dagger_{i\mu}\hat{p}_{i\mu} - 1\right) + \beta_{i0}\left(\sum_\sigma c^\dagger_{i\sigma}c_{i\sigma} - \sum_\mu \hat{p}^\dagger_{i\mu}\hat{p}_{i\mu} - 2\hat{d}^\dagger_i\hat{d}_i\right) \\ &+ \boldsymbol{\beta}_i\cdot\left(\sum_{\sigma\sigma'}\boldsymbol{\tau}_{\sigma\sigma'}c^\dagger_{i\sigma'}c_{i\sigma} - \hat{p}_{i0}\hat{\mathbf{p}}^\dagger_i - \hat{\mathbf{p}}^\dagger_i\hat{p}_{i0} + i(\hat{\mathbf{p}}^\dagger_i\times\hat{\mathbf{p}}_i)\right)\Bigg]. \end{aligned} \tag{A35}$$

Here, the $U_s\hat{d}^\dagger_i\hat{d}_i$ operator equals to the $U_s\hat{n}_{si\uparrow}\hat{n}_{si\downarrow}$ under the constraints (A31).

To perform the saddle-point approximation, we assume the magnetization is in the X-Y plane and takes the form of $\mathbf{M}_i = M\hat{\mathbf{n}}_i$, where $\hat{\mathbf{n}}_i = (\cos\phi_i, \sin\phi_i, 0)$, and $\phi_i = \mathbf{Q}\cdot\mathbf{R}_i$ is site-dependent angle. To describe such magnetization in the mean-field theory, we assume that the vector slave-boson order parameter has the same spatial variation as M_i, so $\mathbf{p}_i = p\hat{\mathbf{n}}_i$, $\boldsymbol{\beta}_i = \beta\hat{\mathbf{n}}_i$. On the other hand, the scalar fields e_i, p_{0i}, α_i, β_{0i} are assumed to be uniform in real space and $d_i = 0$ since U_s is infinitely large. We also assume that all the mean fields are real numbers. The matrix $\sqrt{2}\underline{\hat{p}}_i$ which is defined as $\hat{p}_{\sigma\sigma'} = \frac{1}{2}\sum_{\mu=0}^{3}\hat{p}_\mu\tau_{\mu,\sigma\sigma'}$ has eigenvalues $p_\nu = (p_0 + \nu p)/\sqrt{2}$ and eigenvectors $\chi^\nu_i = \frac{1}{\sqrt{2}}[\nu e^{-i\phi_i}, 1]^T$ with $\nu = \pm 1$. The matrix $\underline{z}_i$, which is defined as

$$\hat{\underline{z}}_i = \hat{e}^\dagger_i\underline{L}_i\underline{R}_i\hat{\underline{p}}_i + \hat{\underline{p}}^\dagger_i\underline{L}_i\underline{R}_i\hat{d}_i, \tag{A36}$$

with

$$\begin{aligned} \underline{L}_i &= [(1 - \hat{d}^\dagger_i\hat{d}_i)\underline{1} - 2\underline{\hat{p}}^\dagger_i\underline{\hat{p}}_i]^{-\frac{1}{2}}, \\ \underline{R}_i &= [(1 - \hat{e}^\dagger_i\hat{e}_i)\underline{1} - 2\underline{\hat{p}}^\dagger_i\underline{\hat{p}}_i]^{-\frac{1}{2}}, \end{aligned} \tag{A37}$$

can be easily evaluated by writing the $\underline{\hat{p}}_i$ matrix as $\sum_\nu p_\nu\chi^\nu_i\chi^{\nu\dagger}_i/\sqrt{2}$:

$$\underline{z}_i = \begin{bmatrix} z_+ & z_-e^{-i\phi_i} \\ z_-e^{i\phi_i} & z_+ \end{bmatrix}. \tag{A38}$$

Here, we have

$$\begin{aligned} z_\pm &= ep_+L_+R_-/\sqrt{2} \pm ep_-L_-R_+/\sqrt{2}, \\ L_\nu &= \left[1 - p^2_\nu\right]^{-\frac{1}{2}}, \quad R_\nu = \left[1 - e^2 - p^2_\nu\right]^{-\frac{1}{2}}. \end{aligned} \tag{A39}$$

Now, we present the Fourier transformation terms in the mean-field Hamiltonian. First, we consider the hopping terms

$t^Y_{s,i,j}$ between s orbitals. From the definition $s_\sigma = \sum_{\sigma'} \hat{z}_{\sigma\sigma'} c_{\sigma'}$, these terms are represented by the pseudofermion operators:

$$\begin{aligned}\sum_{ij\sigma} t^Y_{s,i,j} s^\dagger_{i\sigma} s_{j\sigma} &= \sum_{ij\sigma\sigma_1\sigma_2} t^Y_{s,i,j} z^\dagger_{i\sigma\sigma_1} c^\dagger_{i\sigma_1} c_{j\sigma_2} z_{j\sigma_2\sigma} \\ &= \sum_{ij\sigma_1\sigma_2} \left[\sum_\sigma t^Y_{s,i,j} z^\dagger_{i\sigma\sigma_1} z_{j\sigma_2\sigma}\right] c^\dagger_{i\sigma_1} c_{j\sigma_2} \\ &= \sum_{ij} t^Y_{s,i,j} [c^\dagger_{i\uparrow} c_{j\uparrow} (z_+^2 + z_-^2 e^{i\phi_i - i\phi_j}) + c^\dagger_{i\downarrow} c_{j\downarrow} (z_+^2 + z_-^2 e^{i\phi_j - i\phi_i}) \\ &\quad + c^\dagger_{i\uparrow} c_{j\downarrow} z_+ z_- (e^{i\phi_i} + e^{-i\phi_j}) + c^\dagger_{i\downarrow} c_{j\uparrow} z_+ z_- (e^{-i\phi_i} + e^{i\phi_j})]. \end{aligned} \tag{A40}$$

The fermion operators in k space read as

$$c^\dagger_i = \sum_k e^{ik\cdot R_i} c^\dagger_k, \quad c_i = \sum_k e^{-ik\cdot R_i} c_k. \tag{A41}$$

After Fourier transformation, the t^Y_s hopping terms take the form

$$\begin{aligned}\sum_{ij\sigma} t^Y_{s,i,j} s^\dagger_{i\sigma} s_{j\sigma} &= \sum_{\mathbf{k}} [(z_+^2 t_{\mathbf{k}} + z_-^2 t_{\mathbf{k+Q}}) c^\dagger_{\mathbf{k}\uparrow} c_{\mathbf{k}\uparrow} + (z_-^2 t_{\mathbf{k}} + z_+^2 t_{\mathbf{k+Q}}) c^\dagger_{\mathbf{k+Q}\downarrow} c_{\mathbf{k+Q}\downarrow} \\ &\quad + z_+ z_- (t_{\mathbf{k+Q}} + t_k) c^\dagger_{\mathbf{k}\uparrow} c_{\mathbf{k+Q}\downarrow} + z_+ z_- (t_{\mathbf{k+Q}} + t_{\mathbf{k}}) c^\dagger_{\mathbf{k+Q}\downarrow} c_{\mathbf{k}\uparrow}], \end{aligned} \tag{A42}$$

where the dispersion t_k is defined as $t_{\mathbf{k}} = \epsilon_{s\mathbf{k}} = 2t^Y_s \cos k_Y$ in our model. Further, we give the Fourier transformation of the operators contained in the Lagrangian multiplier into k space:

$$\begin{aligned}\sum_i \boldsymbol{\beta}_i \cdot \boldsymbol{\tau}_{\sigma\sigma'} c^\dagger_{\sigma'} c_\sigma &= \sum_i \beta(\cos\phi_i, \sin\phi_i, 0)(\tau_x, \tau_y, \tau_z)_{\sigma\sigma'} c^\dagger_{i\sigma} c_{i\sigma'} \\ &= \sum_i \beta e^{-i\phi_i} c^\dagger_{i\downarrow} c_{i\uparrow} + \beta e^{i\phi_i} c^\dagger_{i\uparrow} c_{i\downarrow} \\ &= \sum_{i,\mathbf{k},\mathbf{k}'} [\beta e^{i(\mathbf{k}-\mathbf{Q}-\mathbf{k}')\cdot\mathbf{R}_i} c^\dagger_{\mathbf{k}\downarrow} c_{\mathbf{k}'\uparrow} + \beta e^{i(\mathbf{k}+\mathbf{Q}-\mathbf{k}')\cdot\mathbf{R}_i} c^\dagger_{\mathbf{k}\uparrow} c_{\mathbf{k}'\downarrow}] \\ &= \sum_{\mathbf{k}} [\beta c^\dagger_{\mathbf{k+Q}\downarrow} c_{\mathbf{k}\uparrow} + \beta c^\dagger_{\mathbf{k}\uparrow} c_{\mathbf{k+Q}\downarrow}]. \end{aligned} \tag{A43}$$

Finally, we give the Fourier transformation of the hybridization terms into the k space:

$$\begin{aligned}\sum_{i,\mathbf{r},\sigma} F(\mathbf{r}) z^\dagger_{i\sigma\sigma_1} s^\dagger_{i\sigma_1} p_{X,i+\mathbf{r},\sigma} + \text{H.c.} &= \sum_{i,\mathbf{r}} F(\mathbf{r}) [z_+ c^\dagger_{i\uparrow} p_{X,i+\mathbf{r},\uparrow} + z_+ c^\dagger_{i\downarrow} p_{X,i+\mathbf{r},\downarrow}] \\ &\quad + \sum_{i,\mathbf{r}} F(\mathbf{r}) [z_- e^{-i\phi_i} c^\dagger_{i\downarrow} p_{X,i+\mathbf{r},\uparrow} + z_- e^{i\phi_i} c^\dagger_{i\uparrow} p_{X,i+\mathbf{r}\downarrow}] + \text{H.c.} \\ &= \sum_{i,\mathbf{r},\sigma} z_+ F(\mathbf{r}) c^\dagger_{i\sigma} p_{X,i+\mathbf{r},\sigma} + \sum_{\mathbf{k}\mathbf{k}'} \sum_{i,\mathbf{r}} z_- F(\mathbf{r}) e^{i(\mathbf{k}-\mathbf{Q})(\mathbf{R}_i - \mathbf{R}_{i+\mathbf{r}})} e^{-i[\mathbf{k}'-(\mathbf{k}-\mathbf{Q})]\mathbf{R}_{i+\mathbf{r}}} c^\dagger_{\mathbf{k}\downarrow} p_{X\mathbf{k}'\uparrow} \\ &\quad + \sum_{\mathbf{k}\mathbf{k}'} \sum_{i,\mathbf{r}} z_- F(\mathbf{r}) e^{i(\mathbf{k}+\mathbf{Q})(\mathbf{R}_i - \mathbf{R}_{i+\mathbf{r}})} e^{-i[\mathbf{k}'-(\mathbf{k}+\mathbf{Q})]\mathbf{R}_{i+\mathbf{r}}} c^\dagger_{\mathbf{k}\uparrow} p_{X\mathbf{k}'\downarrow} + \text{H.c.} \\ &= \sum_{\mathbf{k}} \Big[z_+ V_{\mathbf{k}} c^\dagger_{\mathbf{k}\uparrow} p_{X\mathbf{k}\uparrow} + z_+ V_{\mathbf{k+Q}} c^\dagger_{\mathbf{k+Q}\downarrow} p_{X\mathbf{k+Q}\downarrow} + z_- V_{\mathbf{k}} c^\dagger_{\mathbf{k+Q}\downarrow} p_{X\mathbf{k}\uparrow} + z_- V_{\mathbf{k+Q}} c^\dagger_{\mathbf{k}\uparrow} p_{X\mathbf{k+Q}\downarrow} \Big] \\ &\quad + \text{H.c.} \end{aligned} \tag{A44}$$

With the above results, we have replaced operators $f^\dagger_{i\sigma}$ with $c^\dagger_{i\sigma}$ and can write the mean-field Hamiltonian in the basis $\mathbf{X}^\dagger_{\mathbf{k}} \equiv (c^\dagger_{\mathbf{k}\uparrow}, c^\dagger_{\mathbf{k+Q}\downarrow}, p^\dagger_{X\mathbf{k}\uparrow}, p^\dagger_{X\mathbf{k+Q}\downarrow})$ as

$$H = \sum_k \mathbf{X}^\dagger_{\mathbf{k}} \epsilon_k \mathbf{X}_{\mathbf{k}} + N\big[-\beta_0\big(p_0^2 + p^2\big) + 2\beta p_0 p + \alpha\big(e^2 + p^2 + p_0^2 - 1\big)\big], \tag{A45}$$

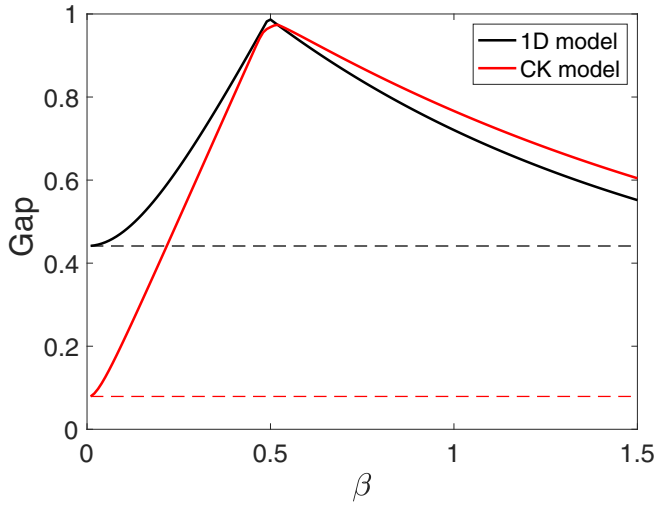

FIG. 11. The band gap versus spontaneous magnetization β in the mean-field Hamiltonian of the simple 1D periodic Anderson model and the CK insulator model, respectively. The dashed lines denote the magnitude of the band gap with $\beta = 0$ in the corresponding models. For the 1D periodic Anderson model, the parameters used are $(z_+v, \epsilon_k) = (0.7, 2\cos k)$, and for the CK model, the parameters are $(t_s^Y, t_p^X, \Delta_s, \phi, t_{sp}, z_+, z_-, \beta_0) = (0.1, 1, 3, 0.5\pi, 0.53, 0.565, 0.358, 2.56)$.

with matrix ϵ_k defined as

$$\epsilon_k = \begin{pmatrix} \epsilon^a_{s\mathbf{k}} + \beta_0 & \epsilon^c_{s\mathbf{k}} + \beta & z_+V_{\mathbf{k}} & z_-V_{\mathbf{k}+\mathbf{Q}} \\ \epsilon^c_{s\mathbf{k}} + \beta & \epsilon^b_{s\mathbf{k}} + \beta_0 & z_-V_{\mathbf{k}} & z_+V_{\mathbf{k}+\mathbf{Q}} \\ z_+V^*_{\mathbf{k}} & z_-V^*_{\mathbf{k}} & \epsilon_{p,\mathbf{k}} & 0 \\ z_-V^*_{\mathbf{k}+\mathbf{Q}} & z_+V^*_{\mathbf{k}+\mathbf{Q}} & 0 & \epsilon_{p,\mathbf{k}+\mathbf{Q}} \end{pmatrix}, \quad \text{(A46)}$$

where $\epsilon^a_{s\mathbf{k}} = z_+^2\epsilon_{s\mathbf{k}} + z_-^2\epsilon_{s\mathbf{k}+\mathbf{Q}} - \Delta_s$, $\epsilon^b_{s\mathbf{k}} = z_+^2\epsilon_{s\mathbf{k}+\mathbf{Q}} + z_-^2\epsilon_{s\mathbf{k}} - \Delta_s$, $\epsilon^c_{s\mathbf{k}} = z_+z_-(\epsilon_{s\mathbf{k}+\mathbf{Q}} + \epsilon_{s\mathbf{k}})$ are s-orbital hopping terms.

5. Effects of the magnetic moment on the band gap

Here, we investigate how the topological band gap is enhanced by the spontaneous magnetization β. We calculate the band gap versus the mean-field order β with all other mean-field parameters being fixed, and find that when β varies from 0 to a large value, the band gap is enhanced and will reach its maximum at intermediate β value. To show the generality of this property, we first consider a simple 1D periodic Anderson model with antiferromagnetic mean-field Hamiltonian

$$H_k^{\mathrm{1D}} = \begin{bmatrix} 0 & \beta & z_+v & 0 \\ \beta & 0 & 0 & z_+v \\ z_+v & 0 & \epsilon_k & 0 \\ 0 & z_+v & 0 & -\epsilon_k \end{bmatrix}, \quad \text{(A47)}$$

which can be directly diagonalized as

$$E_k = \pm\sqrt{\frac{\beta^2 + \epsilon_k^2 + 2(z_+v)^2 \pm \sqrt{\beta^4 - 2\beta^2\epsilon_k^2 + \epsilon_k^4 + 4(z_+v)^2(\beta^2 + \epsilon_k^2)}}{2}}. \quad \text{(A48)}$$

We further show the same phenomenon in our CK model by calculating the band gap with Eq. (29) and antiferromagnetic order, where we also vary the magnetization β but fix other mean-field parameters. The numerical results with specific parameters for the two models are shown in Fig. 11.

[1] M. Dzero, K. Sun, V. Galitski, and P. Coleman, Phys. Rev. Lett. **104**, 106408 (2010).

[2] F. Lu, J. Z. Zhao, H. Weng, Z. Fang, and X. Dai, Phys. Rev. Lett. **110**, 096401 (2013).

[3] V. Alexandrov, M. Dzero, and P. Coleman, Phys. Rev. Lett. **111**, 226403 (2013).

[4] J. W. Allen, B. Batlogg, and P. Wachter, Phys. Rev. B **20**, 4807 (1979).

[5] S. Wolgast, C. Kurdak, K. Sun, J. W. Allen, D.-J. Kim, and Z. Fisk, Phys. Rev. B **88**, 180405 (2013).

[6] D. J. Kim, S. Thomas, T. Grant, J. Botimer, Z. Fisk, and J. Xia, Sci. Rep. **3**, 3150 (2013).

[7] D. J. Kim, J. Xia, and Z. Fisk, Nat. Mater. **13**, 466 (2014).

[8] J. Jiang, S. Li, T. Zhang, Z. Sun, F. Chen, Z. Ye, M. Xu, Q. Ge, S. Tan, X. Niu *et al.*, Nat. Commun. **4**, 3010 (2013).

[9] M. Neupane, N. Alidoust, S.-Y. Xu, T. Kondo, Y. Ishida, D. J. Kim, C. Liu, I. Belopolski, Y. J. Jo, T.-R. Chang *et al.*, Nat. Commun. **4**, 2991 (2013).

[10] N. Xu, X. Shi, P. K. Biswas, C. E. Matt, R. S. Dhaka, Y. Huang, N. C. Plumb, M. Radovic, J. H. Dil, E. Pomjakushina *et al.*, Phys. Rev. B **88**, 121102 (2013).

[11] E. Frantzeskakis, N. de Jong, B. Zwartsenberg, Y. K. Huang, Y. Pan, X. Zhang, J. X. Zhang, F. X. Zhang, L. H. Bao, O. Tegus *et al.*, Phys. Rev. X **3**, 041024 (2013).

[12] N. Xu, P. K. Biswas, J. H. Dil, G. Landolt, S. Muff, C. E. Matt, X. Shi, N. C. Plumb, M. Radavic, E. Pomjakushina, K. Conder, A. Amato, S. V. Borisenko, R. Yu, H.-M. Weng, Z. Fang, X. Dai, J. Mesot, H. Hing, and M. Shi, Nat. Commun. **5**, 4566 (2014).

[13] W. Ruan, C. Ye, M. Guo, F. Chen, X. Chen, G.-M. Zhang, and Y. Wang, Phys. Rev. Lett. **112**, 136401 (2014).

[14] S. Roessler, T.-H. Jang, D.-J. Kim, L. H. Tjeng, Z. Fisk, F. Steglich, and S. Wirth, Proc. Natl. Acad. Sci. USA **111**, 4798 (2014).

[15] O. Erten, P.-Y. Chang, Piers Coleman, and Alexei M. Tsvelik, Phys. Rev. Lett. **119**, 057603 (2017).

[16] G. Li, Z. Xiang, F. Yu, T. Asaba, B. Lawson, P. Cai, C. Tinsman, A. Berkley, S. Wolgast, Y. S. Eo, D.-J. Kim, C. Kurdak, J. W.

Allen, K. Sun, X. H. Chen, Y. Y. Wang, Z. Fisk, and L. Li, Science **346**, 1208 (2014).
[17] B. S. Tan, Y.-T. Hsu, B. Zeng, M. C. Hatnean, N. Harrison, Z. Zhu, M. Hartstein, M. Kiourlappou, A. Srivastava, M. D. Johannes, T. P. Murphy, J.-H. Park, L. Balicas, G. G. Lonzarich, G. Balakrishnan, and S. E. Sebastian, Science **349**, 287 (2015).
[18] K. Flachbart, M. Reiffers, and S. Janos, J. Less-Common Met. **88**, L11 (1982).
[19] Y. Xu, S. Cui, J. K. Dong, D. Zhao, T. Wu, X. H. Chen, K. Sun, H. Yao, and S. Y. Li, Phys. Rev. Lett. **116**, 246403 (2016).
[20] N. J. Laurita, C. M. Morris, S. M. Koohpayeh, P. F. S. Rosa, W. A. Phelan, Z. Fisk, T. M. McQueen, and N. P. Armitage, Phys. Rev. B **94**, 165154 (2016).
[21] M. Hartstein *et al.*, Nat. Phys. **14**, 166 (2017).
[22] J. Iaconis and L. Balents, Phys. Rev. B **91**, 245127 (2015).
[23] V. Alexandrov and P. Coleman, Phys. Rev. B **90**, 115147 (2014).
[24] V. Alexandrov, P. Coleman, and O. Erten, Phys. Rev. Lett. **114**, 177202 (2015).
[25] R. Peters, T. Yoshida, H. Sakakibara, and N. Kawakami, Phys. Rev. B **93**, 235159 (2016).
[26] A. Thomson and S. Sachdev, Phys. Rev. B **93**, 125103 (2016).
[27] A. Mezio, A. M. Lobos, A. O. Dobry, and C. J. Gazza, Phys. Rev. B **92**, 205128 (2015).
[28] F. T. Lisandrini, A. M. Lobos, A. O. Dobry, and C. J. Gazza, Phys. Rev. B **96**, 075124 (2017).
[29] S. Ok, Markus Legner, Titus Neupert, and Ashley M. Cook, arXiv:1703.03804.
[30] H. Chen, X.-J. Liu, and X. C. Xie, Phys. Rev. Lett. **116**, 046401 (2016).
[31] C. Zhang, S. Tewari, R. M. Lutchyn, and S. Das Sarma, Phys. Rev. Lett. **101**, 160401 (2008).
[32] M. Sato, Y. Takahashi, and S. Fujimoto, Phys. Rev. Lett. **103**, 020401 (2009).
[33] X.-J. Liu, X. Liu, C. Wu, and J. Sinova, Phys. Rev. A **81**, 033622 (2010).
[34] N. Goldman, I. Satija, P. Nikolic, A. Bermudez, M. A. Martin-Delgado, M. Lewenstein, and I. B. Spielman, Phys. Rev. Lett. **105**, 255302 (2010).
[35] S.-L. Zhu, L. B. Shao, Z. D. Wang, and L.-M. Duan, Phys. Rev. Lett. **106**, 100404 (2011).
[36] X.-J. Liu, K. T. Law, and T. K. Ng, Phys. Rev. Lett. **112**, 086401 (2014); **113**, 059901(E) (2014).
[37] N. Goldman, G. Juzeliūnas., P. Öhberg, and I. B. Spielman, Rep. Prog. Phys. **77**, 126401 (2014).
[38] H. Zhai, Rep. Prog. Phys. **78**, 026001 (2015).
[39] W. Yi, W. Zhang, and X. L. Cui, Sci. China Phys. Mech. Astron. **58**, 1 (2015).
[40] X. Li and W. V. Liu, Rep. Prog. Phys. **79**, 116401 (2016).
[41] L. Zhang and X.-J. Liu, Spin-orbit coupling and topological phases for ultracold atoms, in *Synthetic Spin-orbit Coupling in Cold Atoms* (World Scientific, Singapore, 2018), Chap. 1, pp. 1–87.
[42] L.-F. Guo, P. Li, and S. Yi, Phys. Rev. A **95**, 063610 (2017).
[43] Y. Deng, R. Lü, and L. You, Phys. Rev. B **96**, 144517 (2017).
[44] X.-H. Li, T.-P. Choy, and T.-K. Ng, Phys. Rev. A **95**, 033628 (2017).
[45] Z. Zheng *et al.*, New J. Phys. **20**, 023039 (2018).
[46] B. Song, L. Zhang, C. He, T.-F. J. Poon, E. Hajiyev, S. Zhang, X.-J. Liu, and G.-B. Jo, Sci. Adv. **4**, eeao4748 (2018).
[47] S. Zhang and G.-B. Jo, J. Phys. Chem. Solids (2018), doi: 10.1016/j.jpcs.2018.04.033.
[48] L. Zhang, L. Zhang, S. Niu, and X.-J. Liu, arXiv:1802.10061v2.
[49] W. Sun, C.-R. Yi, B.-Z. Wang, W.-W. Zhang, B. C. Sanders, X.-T. Xu, Z.-Y. Wang, J. Schmiedmayer, Y. Deng, X.-J. Liu, S. Chen, and J.-W. Pan, arXiv:1804.08226.
[50] P. O. Fedichev, Y. Kagan, G. V. Shlyapnikov, and J. T. M. Walraven, Phys. Rev. Lett. **77**, 2913 (1996).
[51] F. K. Fatemi, K. M. Jones, and P. D. Lett, Phys. Rev. Lett. **85**, 4462 (2000).
[52] M. Theis, G. Thalhammer, K. Winkler, M. Hellwig, G. Ruff, R. Grimm, and J. H. Denschlag, Phys. Rev. Lett. **93**, 123001 (2004).
[53] K. Enomoto, K. Kasa, M. Kitagawa, and Y. Takahashi, Phys. Rev. Lett. **101**, 203201 (2008).
[54] D. M. Bauer, M. Lettner, C. Vo, G. Rempe, and S. Dürr, Nat. Phys. **5**, 339 (2009).
[55] S. Blatt, T. L. Nicholson, B. J. Bloom, J. R. Williams, J. W. Thomsen, P. S. Julienne, and J. Ye, Phys. Rev. Lett. **107**, 073202 (2011).
[56] L. W. Clark, L.-C. Ha, C.-Y. Xu, and C. Chin, Phys. Rev. Lett. **115**, 155301 (2015).
[57] M. Aidelsburger, M. Atala, S. Nascimbène, S. Trotzky, Y.-A. Chen, and I. Bloch, Phys. Rev. Lett. **107**, 255301 (2011).
[58] M. Aidelsburger, M. Atala, M. Lohse, J. T. Barreiro, B. Paredes, and I. Bloch, Phys. Rev. Lett. **111**, 185301 (2013).
[59] H. Miyake, G. A. Siviloglou, C. J. Kennedy, W. C. Burton, and W. Ketterle, Phys. Rev. Lett. **111**, 185302 (2013).
[60] J. Struck *et al.*, Nat. Phys. **9**, 738 (2013).
[61] S. Doniach, Physica B&C (Amsterdam) **91**, 231 (1977).
[62] B. Möller and P. Wölfle, Phys. Rev. B **48**, 10320 (1993).
[63] R. Doradziński and J. Spałek, Phys. Rev. B **56**, R14239 (1997); **58**, 3293 (1998).
[64] V. Dorin and P. Schlottmann, Phys. Rev. B **46**, 10800 (1992).
[65] M. Guerrero and Clare C. Yu, Phys. Rev. B **51**, 10301 (1995).
[66] X.-J. Liu, Z.-X. Liu, K. T. Law, W. V. Liu, and T. K. Ng, New J. Phys. **18**, 035004 (2016).
[67] J. R. Schrieffer and P. A. Wolff, Phys. Rev. **149**, 491 (1966).
[68] Y. Kakehashi, *Modern Theory of Magnetism in Metals and Alloys* (Springer, Berlin, 2013), Chap. 7.
[69] Z. Xiong and X.-G. Wen, arXiv:1208.1512.
[70] P. Coleman, Phys. Rev. B **29**, 3035 (1984).
[71] G. Kotliar and A. E. Ruckenstein, Phys. Rev. Lett. **57**, 1362 (1986).
[72] Martin C. Gutzwiller, Phys. Rev. **137**, A1726 (1965).
[73] T. Li, P. Wölfle, and P. J. Hirschfeld, Phys. Rev. B **40**, 6817 (1989); R. Frésard and P. Wölfle, Int. J. Mod. Phys. B **6**, 685 (1992); **6**, 3087(E) (1992).
[74] R. Frésard and P. Woölfle, J. Phys.: Condens. Matter **4**, 3625 (1992).
[75] C. Pépin, Phys. Rev. B **77**, 245129 (2008).
[76] D. M. Newns and N. Read, Adv. Phys. **36**, 799 (1987).
[77] S. Doniach and E. H. Sondheimer, *Green's Functions for Solid State Physicists* (Benjamin, New York, 1974).
[78] G. Jotzu, M. Messer, R. Desbuquois, M. Lebrat, T. Uehlinger, D. Greif, and T. Esslinger, Nature (London) **515**, 237 (2014).
[79] R. Jördens, N. Strohmaier1, K. Günter, H. Moritz, and T. Esslinger, Nature (London) **455**, 204 (2008).
[80] S. Taie, R. Yamazaki, S. Sugawa, and Y. Takahashi, Nat. Phys. **8**, 825 (2012).